Received: 20 August 2024 | Accepted: 10 April 2025

DOI: 10.1002/vzj2.70021

Vadose Zone Journal

ORIGINAL ARTICLE

Dynamic soil water retention properties: Exploring the interplay of moisture states and soil structure dynamics in a compacted Andosol

Sebastián Bravo Peña[1,2] | **Loes van Schaik**[1] | **José Dörner**[2,3] | **Jos van Dam**[1]

[1]Department of Soil Physics and Land Management (SLM), Wageningen University & Research, Wageningen, The Netherlands

[2]Institute of Agricultural Engineering and Soils (IIAS), Faculty of Agricultural and Food Science, Austral University of Chile, Valdivia, Chile

[3]Research Centre on Volcanic Ash Soils (CISVo), Universidad Austral de Chile, Valdivia, Chile

Correspondence
Sebastián Bravo Peña, Department of Soil Physics and Land Management, Wageningen University & Research, Postal address: PO Box 47; 6700 AA Wageningen, The Netherlands.
Email: sebastian.bravopena@wur.nl

Assigned to Associate Editor Quirijn de Jong van Lier.

Funding information
Agencia Nacional de Investigación y Desarrollo (ANID), Grant/Award Number: Beca Chile/2019-72200251; Dutch Research Council (NWO), Grant/Award Number: OCENW.M.22.375; Fondo Nacional de Desarrollo Científico y Tecnológico (FONDECYT), Grant/Award Number: 1191057

Abstract

The influence of soil structure dynamics on spatiotemporal variability in soil water flows and distribution is generally omitted in hydrological modeling across scales. Soils like Andosols exhibit important structural dynamics, which affects the accurate representation of soil water distribution and solute transport. This study aimed to describe spatiotemporal variability of soil water retention (SWR) functions in a variably compacted Andosol. Laboratory and field observations were conducted at 10-, 20-, and 60-cm depths in a grassland in southern Chile. We studied 10-min resolution time series from 48 soil moisture contents and 18 matric potential sensors across six monitoring stations from June 2020 to June 2022. Wet and dry period dynamics were delineated based on soil moisture states. Wetting/drying cycles were identified using time derivatives of soil moisture content. Unimodal (vG) and bimodal (dualvG) formulations of the van Genuchten equation were fitted. This study provides insights into how soil structural dynamics, as affected by variable water-filled pore volumes, influence the SWR parameters across different compaction levels and depths. Laboratory and field observations represented different conditions, describing expected contrasts. The dualvG performed better than vG for lab data, showing lower Akaike information criterion (AIC) and root mean squared error (RMSE), and high R^2. Soil compaction influenced the dualvG parameters and decreased the diversity of field SWR behavior. Wetting and drying cycles did not affect model parameters. However, it allowed for describing peaks of homogeneity and heterogeneity when wet and dry period dynamics were considered. Non-systematic hysteretic behaviors in the data suggested the occurrence of non-uniform flows.

Abbreviations: PF, preferential flow; SWRC, soil water retention curve; vG, van Genuchten equation; VWC, volumetric water content.

Plain Language Summary

This research focuses on how the soil pore structure and moisture state variations over time and at different depths in a compacted volcanic ash soil affect the soil water retention (SWR) characteristics. We aimed to understand this interplay by analyzing soil moisture and tension data collected in different soil layers every 10 min over two years in a grassland. We found that compacted soils affected some SWR parameters and showed less variability in SWR data because of soil pores degradation. However, this led to more extreme SWR behaviors. During wet periods, the water distribution was mostly uniform, while dry periods showed uniform drying but highly variable wetting cycles. Wetting and drying cycles did not affect model parameters. Understanding the dynamics of soil pore structures is crucial for accurately representing soil water properties and distribution.

1 | INTRODUCTION

The heterogeneity of soil hydraulic properties across different spatial and temporal scales leads to complex subsurface water flows, making it challenging to predict soil water distribution and solute transport (Beven & Germann, 2013; N. Jarvis et al., 2016; Vereecken et al., 2022). Soil water is influenced by highly nonlinear interactions within the soil–plant–atmosphere continuum. At the pore scale, water flow through diverse pore networks creates variable relationships between water contents and retention forces. This is known as hysteresis and has been researched for almost a century (Haines, 1930). This phenomenon depicts variation in the water retention function depending on the initial soil moisture state and the following wetting or drying process (Basile et al., 2003; Diamantopoulos et al., 2012; Poulovassilis, 1962).

To describe soil water status in porous media, the soil water retention curve (SWRC) is widely used. The SWRC provides valuable information about pore-size distribution, water storage, plant-available water, and soil air capacity (Hartge et al., 2016). To fit this function mathematically, a diversity of analytical equations can be used (Brooks & Corey, 1966; Kosugi, 1996; van Genuchten, 1980). Generally, the water retention properties are represented by a single and time-invariant SWRC, being the unimodal van Genuchten (vG) equation (van Genuchten, 1980) one of the most recognized in hydrological modeling. This representation is valid under non-hysteretic hydraulic equilibrium conditions, meaning that a moisture content observation represents a unique matric potential at every point and direction along this function (Hannes et al., 2016; Vogel et al., 2023). This model overlooks possible temporal dynamics in soil physical properties or flow phenomena commonly observed under field conditions. Nevertheless, due to its compatibility with the theories of Mualem (1976) and Burdine (1953), the unimodal vG model and its closed-form conductivity functions have been widely and successfully used in hydrological studies across scales. Even though its original form is non-hysteretic, this model can be accurately fitted to observations along individual wetting or drying processes (van Genuchten, 1980), resembling a pseudo-hysteresis approach.

When soils exhibit a more structured pore system, several inflection points can be found along the SWRC, representing hierarchical aggregation between primary and secondary pore systems (Dörner et al., 2010). To account for this, the pore-size distribution can be characterized by bimodal or multimodal SWRCs. Similarly to other numerical solutions, the vG equation was adapted to integrate multiple weighted subfunctions, producing more complex curvatures to represent water retention in structured soils (Durner, 1994). Water distribution in the unsaturated zone exhibits complex behavior due to both uniform and preferential flows dynamically occur under several circumstances. The occurrence of preferential flow (PF) depends on several factors, such as precipitation frequency and intensity, land cover and roots spatial configuration, soil water repellency, initial soil moisture state (Blume et al., 2009; N. Jarvis et al., 2016; Nimmo, 2021), or mechanical stresses such as soil compaction (Kulli et al., 2003). This leads to spatial and temporal heterogeneity in the soil moisture distribution (N. Jarvis et al., 2016), and therefore, variability in the water retention properties described by continuous field observations. This spatiotemporal variability, and its influence on the derivation of appropriate SWRCs, has been a persistent challenge for soil hydrologists (Basset et al., 2023; Beck-Broichsitter et al., 2023; N. Jarvis et al., 2024; Vereecken et al., 2022; Vogel et al., 2023; Wang et al., 2023).

Soil structure dynamics are an important omission in Earth system models (Fatichi et al., 2020). Recently, efforts have been made to quantify their hydrological effects across

spatial and temporal scales (Bonetti et al., 2021; N. Jarvis et al., 2024). At the catchment scale, soil properties contribute to the spatiotemporal variability of soil water between wet and dry periods (Hendrickx et al., 2023; Rosenbaum et al., 2012). At plot scale, natural processes such as soil shrinkage/swelling cause dynamics in soil structure (Dörner et al., 2009; Horn et al., 2014; Peng & Horn, 2005) and thereby spatial and temporal variability in SWR. Although one might assume a more homogenized system in agricultural soils, continuous field observations on SWR describe temporal variations as affected by agricultural management (e.g., type of tillage) and growing seasons (Huang et al., 2021; Pečan et al., 2023; Zhang et al., 2017). These studies provided evidence of temporal dynamics in SWR capacity, primarily focusing on the drying processes. However, studies on temporal dynamics of SWR parameters during wetting and drying cycles using high-resolution continuous field observations are scarce. Moreover, little is known about how field SWR dynamics are affected by the functional degradation of soil pores and its subsequent influence on soil water distribution.

Realistic soil hydraulic properties might then be described by dynamic functions that could represent the system's temporal behaviors as influenced by environmental patterns. Hannes et al. (2016) accurately described SWR dynamics using different hysteresis models. Nevertheless, the incorporation of time-domain information on the environmental conditions to discern when these dynamics are likely to occur remains understudied. N. Jarvis et al. (2016) accurately anticipated that model parameterization would remain a major challenge in soil hydrology. More recently, researchers have stressed the need for a new generation of pedo-transfer functions to address the complexity of temporal variations of soil properties and flow phenomena (Vereecken et al., 2022; Weber et al., 2024).

In our study, we hypothesize that both temporal changes in pore space—driven by soil structure dynamics and compaction—and the variability of soil water distribution influence the temporal dynamics of SWR points observed in the field, and consequently, the derived soil water retention parameters. To assess temporal variations, in SWRCs, we studied wetting and drying cycles over 2 years and analyzed the effect of contrasting water-filled pore volumes during wetter and drier seasons dynamics. To account for different soil structure conditions, monitored soil moisture content and potential were studied under three different degrees of soil compaction. We additionally hypothesize that soil-pore functional degradation due to compaction decreases the diversity of active pore networks, impacting the soil water distribution and thereby the SWR observations. Particularly, we aim to describe the impacts of spatiotemporal variability of continuous field observations on widely used equilibrium-based SWR functions using a dual-porosity approach.

Core Ideas

- Soil water retention variability is temporally dynamic in agricultural grasslands.
- Aligning the process and observation scales is key to recognizing heterogeneous flows.
- Soil structure and water distribution dynamically shape soil water retention functions.
- Soil compaction decreases the diversity of possible scanning curves.
- The collapse of pore networks provokes extreme nonequilibrium relations.

2 | METHODS

2.1 | Study area

The Universidad Austral de Chile's experimental field station (Estación Experimental Agropecuaria Austral [EEAA], 39° 46′ S, 73° 13′ W, 12 m.a.s.l.) is in Valdivia city, southern Chile. This area is under a humid-temperate climate with a mean annual temperature of 12°C and a mean annual precipitation of 2440 mm between 1901 and 2005 (González-Reyes & Muñoz, 2013). The soil corresponds to a volcanic ash-derived soil classified as Petroduri-Silandic Andosol (WRB, 2014), which describes strong structural dynamics (Dörner et al., 2022). Bravo et al. (2020) presented a morphological description of the soil profile until 200-cm depth. In the upper 38 cm (Ap and B1 horizons), clay content is around 29%. This content decreases to 12% in the next 38 to 57 cm (B2 horizon) and consecutively increases to 30% between 57- and 93-cm depth (B3 horizon). Finally, it decreases to 10% at 203-cm depth (2BCE horizon). The soil presents a large amount of organic matter that varies from 12.7% (Ap horizon) to 2.9% (2BCE horizon). The soil bulk density (Bd) ranged from 0.79 (Ap horizon) to 0.56 g cm^{-3} at the deepest layer (2BCE horizon). The topography in the area is highly variable, with dominant slopes from 3% to 8%.

The experimental site belongs to the research project FONDECYT 1191057: "Assessing the effect of the physico-chemical quality of a volcanic ash soil on pasture productivity and soil resilience capacity." A set of six monitoring stations collected high-resolution observations of soil–water state variables since September 2019. Plots of 1728 m^2 with three different compaction levels (T0: Bd = 0.65 g cm^{-3}, T1: Bd = 0.75 g cm^{-3}, and T2: Bd = 0.85 g cm^{-3}) were established using rollers (two types: 1.20 and 1.37 Mg over working widths of 3 and 6 m, respectively) to assess the soil physical degradation of pore functional properties. The vegetation over the experimental area is a sown diverse pasture which includes

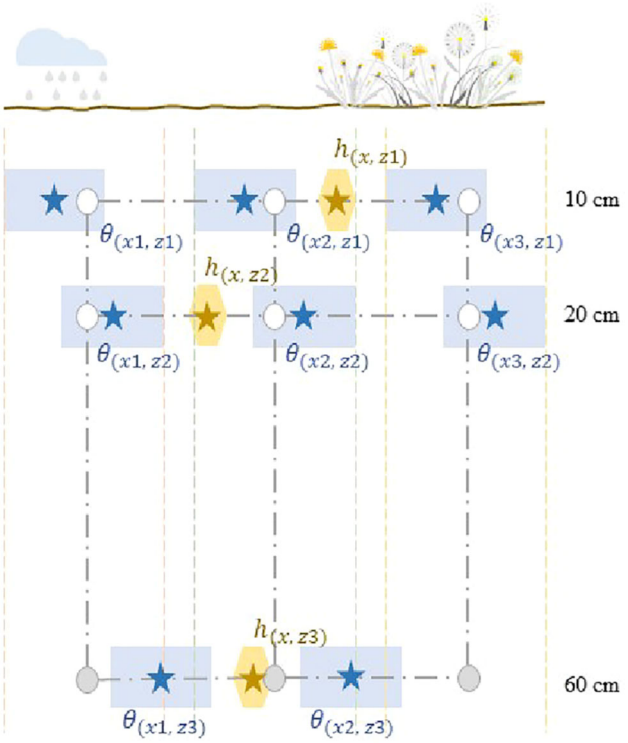

FIGURE 1 Schematic overview of soil moisture (blue stars) and matric potential (light-brown starts) sensors location and their integration volume (squares and hexagons, respectively) at each monitoring station. Circles represent a designed grid where nodes with observed (white) and estimated (gray) values can be assigned in two-dimensional representations. The horizontal distance between nodes is 45 cm.

Lolium perenne, *Trifolium repens*, *Festuca arundinacea*, *Holcus lanatus*, *Dactilys glomerata*, and *Bromus valdivianus*. A detailed description of the experimental design and the agricultural managements can be found in Dörner et al. (2022, 2023).

2.2 | Soil water and environmental variables time series

The study of 2-year soil moisture dynamics (June 1, 2020 to June 1, 2022, 10-min resolution, N = 105,121 observations) used six monitoring stations; two were located at each compaction treatment (Dörner et al., 2022). Within the compaction treatments, these two stations are located in differently fertilized plots. Nevertheless, we do not expect substantial impact from fertilization as it started during the last quarter of the studied period. Since our focus is on soil physical dynamics, monitoring stations will be referred to as Station 1 and Station 2. Each monitoring station (Figure 1) is provided with eight soil moisture sensors (TEROS 11, METER Group; resolution: 0.001 m^3 m^{-3}, range: 0.00–0.70 m^3 m^{-3}) installed at 10-, 20-, and 60-cm depth. The number of TEROS 11 sensors per depth are 3, 3, and 2, respectively. At each depth, one soil matrix potential sensor (TEROS 21 Gen 1, METER Group; resolution: 0.01 kPa, range: ≈−9 to −100,000 kPa) is also installed. The air entry potential of the largest pores in the ceramic of sensors TEROS 21 is about −9 kPa, which may have two main consequences: (i) the sensor might not respond in case the soil has a lower (more negative) air-entry potential than the sensor's ceramic and (ii) it limits the measurement from ≈−9 kPa toward full saturation (wet-end). On the one hand, we believe the soil's air-entry value would not affect the measurements since it increases (less negative) in well-structured soils with very high total porosity (>60%) as Andosols. For more details, Dörner et al. (2022) measured field air permeability and air capacity (at −6 kPa) at the experiment site. On the other hand, near saturation conditions were not reached due to the constant drainage and high-hydraulic conductivity of these soils. After examining the time series over the wettest conditions, observations of pressure head vary according to the VWC dynamics. The latest did not reach saturation levels such as the ones determined at the laboratory (θ_s > 0.64 m^3 m^{-3}). We did not find a lack of response from the sensor, suggesting that the range of our observations is not affected by the wet-end limitations provided by the manufacturer (Figure S1).

All data were recorded by dataloggers in a raw form. Since no facilities were available for the calibration of TEROS 21 over its entire range, matric potential raw data were transformed to kPa unit using the manufacturer calibration. Water content raw data were transformed to soil water content (m^3 m^{-3}) by using a gravimetric calibration for each soil depth (Dec et al., 2022). The volumetric water content (VWC, %) was used in this research.

The time scale attributes of in-situ observations at each monitoring station are composed of (i) 2-year temporal extent and (ii) 10-min resolution. The spatial scale attributes at each monitoring station cover a two-dimensional soil profile (≈0.7 m^2, Figure 1), and the integration volume/area at each sensor location is 1000 cm^3 for VWC and ≈16 cm^2 contact area (at the two faces of the sensor disks) for pressure head.

Since only one replicate of TEROS 21 is available per depth, VWC observations from three TEROS 11 per depth were averaged at each time step, resulting in a one-dimensional vertical profile. Following the filtering scheme and data processing recommendations from Hannes et al. (2015), a smoothing routine was conducted to both VWC and pressure head observations. We manually discarded outliers as well as decreased the noise in the time series by (i) correcting observations based on the sensors resolution and (ii) applying a moving average with a seven-observation window (considering 30 min before and after the central observation). Precipitation (P) measurements were collected by a high-resolution rain gauge (ECRN-100, METER Group; 0.2-mm

resolution) located in the experimental field. The accumulated P for 2020 and 2021 were particularly low compared to the historical mean, being 1682 and 1410 mm, respectively. Reference Evapotranspiration (ET_0, mm day^{-1}) data were consulted from the online agrometeorological monitoring network repository: "Red de Estaciones Agrometeorológicas de INIA" (https://agrometeorologia.cl), using the "Austral" station, located in the EEAA experimental field. The accumulated ET_0 for 2020 and 2021 were 786 and 833 mm, respectively.

2.3 | Soil hydraulic properties in laboratory conditions

2.3.1 | Soil hydraulic functions and derived pore-size distribution

The data were provided by the project FONDECYT 1191057. The laboratory soil water retention curves ($SWRC_{lab}$) were measured over main drying curves using undisturbed soil samples in stainless steel cylinders ($v = 230$ cm^3, $h = 5.6$ cm, $\phi = 7.2$ cm). Describing wetting curves over a wide range of matric potentials in Andosols was not performed since it is practically difficult. Due to their high organic matter content and shrinkage capacity, soil samples generally show irreversible changes in soil volume after exposed to extreme hydraulic stress. The samples ($n = 7$ for each depth) were collected at the site of each monitoring station during their installation and were carefully saturated from beneath. Subsequently, samples were equilibrated and weighed (on an electronic balance, Precisa, 0.01 g accuracy) at the following pressure heads: 0, −1, −2, −3, and −6 kPa (in sand boxes) and −15 and −33 kPa (in pressure chambers). Each sample height was measured in five points (using a Vernier Caliper, 0.001 mm accuracy) to correct the VWC due to shrinkage (Dörner et al., 2015). To determine the permanent wilting point (θ_{PWP}) and the fine pores volume, samples ($n = 5$) of 20 cm^3 were equilibrated at −1543 kPa (in a pressure chamber).

The pore-size classes consist of structural pores as macropores (MaP: $h \geq -1$ kPa) and wide coarse pores (wCP: $-1 > h \geq -6$ kPa), textural pores as the narrow coarse pores (nCP: $-6 > h \geq -33$ kPa), available water pores as the medium pores (MP: $-33 > h > -1543$ kPa), and fine pores (FP: $h \leq -1543$ kPa) following Beck-Broichsitter et al. (2020). To define the VWC, the samples were first weighted and then oven-dried at 105°C for 24 h to calculate the bulk density.

The scale triplet attributes of our laboratory samples collected per depth at each of the six monitoring stations are then composed of (i) 1-m^2 spatial extent, (ii) 10–20 cm random spacing between seven samples per depth, and (iii) 230 cm^3 total volume of each undisturbed soil sample.

2.4 | Soil hydraulic properties at field conditions

2.4.1 | Defining wet and dry period dynamics

The temporal variation of soil moisture states presents a bimodal distribution as a result of land surface–atmosphere feedback (Eagleson, 1994). Since soil hydraulic properties are influenced by these states, a straightforward alternative to shed light on the time-variable behavior is assessing soil wetting and drying processes at different water-filled pore volumes. Therefore, we defined wet and dry period dynamics focused on the soil moisture observations.

Due to more intense moisture dynamics taking place toward the surface, directly influencing the infiltration process to deeper layers, the present research used the mean VWC (θ_μ) at 10-cm depth (with the time series length being the total number of observations N) to determine the transition between wet and dry dynamics. This way, any observation $\theta_i \geq \theta_\mu$ remaining longer than a certain time length threshold (τ) is defined as part of a wet period (WP) dynamic. When a wetting cycle during a WP ends, the observations measured along the subsequent drying cycle remain assigned to the WP until $\theta_i < \theta_\mu$. After separating all WP dynamics, the remaining wetting cycles beginning at $\theta_i < \theta_\mu$ are consequently defined as part of a dry period (DP) dynamic. For this case, as the peaks of moisture increment surpass the θ_μ and remain over it for a time shorter than a set threshold ($\Delta t < \tau$), the observations along the wetting and subsequent drying cycle starting at $\theta_i > \theta_\mu$ are considered part of the DP. Considering a VWC observation in a specific time θ_t, the abovementioned conditions are defined as follows:

$$Period = \begin{cases} \theta_{t+1} = WP & if\ \theta_t \geq \theta_\mu\ AND\ \theta_{[(t-\tau):t]} \geq \theta_\mu \\ \theta_{t+1} = DP & otherwise. \end{cases}, \quad (1)$$

where $\theta_{[(t-\tau):t]}$ represents a consecutive sequence of observations with a length τ preceding the evaluated θ_t. In our research, $\tau = 10$ days was enough to discriminate the peaks of soil moisture occurring during the dry periods when high precipitation events took place. To simplify the conditions in the present approach, the transition point ($\theta_i = \theta_\mu$) was considered part of WP dynamics since we are evaluating a humid-temperate condition.

Once VWC dynamics are separated, the shape of WP and DP data sets distributions were analyzed using the general probability density function (pdf, Equation 2), which is formally written as follows:

$$P\left[\theta_0 < \theta_i \leq \theta_1\right] = \int_{\theta_0}^{\theta_1} f(\theta)\, d\theta = 1, \quad (2)$$

where θ_i is a VWC observation within a DP or WP. The terms θ_0 and θ_1 are the extremes of the cumulative distribution function of VWC, $f(\theta)$, corresponding to the values 0 and 1.

2.4.2 | Separating wetting and drying processes

Since the soil water retention dynamics vary along wetting and drying cycles, resulting in soil hydraulic properties changes both at laboratory and field conditions (Bodner et al., 2013), the time derivative of the volumetric water content (Equation 3) was used to define these cycles as follows:

$$Cycle = \begin{Bmatrix} \theta_t = \text{Wetting} & if\ \theta_{t+1} - \theta_t > 0 \\ \theta_t = \text{Drying} & if\ \theta_{t+1} - \theta_t < 0 \\ \theta_t = \text{Transition} & if\ \theta_{t+1} - \theta_t = 0 \end{Bmatrix}. \quad (3)$$

Due to the large number of observations in the high-resolution data set, the abovementioned transition (representing no change in VWC between two consecutive observations in time) was discarded from the parameter estimation.

2.4.3 | Dynamic soil hydraulic functions from field observations

Once time series were divided into WP and DP dynamics, as well as into wetting and drying cycles, observations of VWC (θ_i) and pressure head (h_i) were used to obtain field soil water retention curves ($SWRC_{fld}$). Hereafter, the averaged soil moisture content ($\bar{\theta}$) of the total number of replicates (N) per depth (z) and the respective pressure head (h_z) were used as follows (Equation 4):

$$\begin{gathered} \theta\ (h) = \text{SWRC}_{\text{fld}}\ \left(h, \bar{\theta}\right), \\ h = h_{(x,\, z_n)};\ \ \bar{\theta} = \frac{1}{N}\ \sum_{i=1}^{N} \theta_{(x_n,\, z_n)}\ . \end{gathered} \quad (4)$$

In this way, different functions can describe (i) the influence of the moisture state, also referred to as water-filled pores volume, in wetter and drier conditions, and (ii) the effect of specific soil pore networks during wetting and drying cycles on soil hydraulic properties. Laboratory SWR parameters were derived numerically using unimodal (van Genuchten, 1980) and bimodal (Durner, 1994) solutions, while field SWR parameters were obtained using the bimodal function only. A detailed explanation of the numerical approaches is given in Section 2.5.

2.5 | Modeling approaches for SWRC

To explore the influence of soil structure dynamics and the heterogeneity of water flows during WP and DP dynamics, as well as wetting and drying cycles, we assessed four strategies to derive the soil water retention curve (SWRC; $\theta(h)$):

1. Laboratory observations: unimodal and bimodal parameterization.
2. Field observations: complete time series length with bimodal parameterization.
3. Field observations: wetting and drying cycles with bimodal parameterization.
4. Field observations: dynamic-based bimodal parameterization considering wetting and drying cycles during WP and DP.

2.5.1 | Fitting numerical models to laboratory and field observations

The soil water retention (SWR) functions $\theta(h)$ at laboratory conditions were described using the van Genuchten (vG) model (van Genuchten, 1980) defined as follows (Equations 5–7):

$$\begin{gathered} \theta_i\ (h) = \theta_r + \frac{\theta_s - \theta_r}{\left(1 + |\alpha h|^n\right)^m};\ h < 0 \\ \theta\ (h) = \theta_s;\ h \geq 0 \\ m = 1 - \frac{1}{n}; n > 1, \end{gathered} \quad (5)$$

where θ_r and θ_s represent the residual and saturated volumetric water content ($L^3\ L^{-3}$), respectively, while α (kPa^{-1}) and n [-] are shape parameters. To obtain a relative SWR function, the effective saturation S_e [-] as a function of the pressure head is given by:

$$S_e\,(h) = \frac{\theta_i\,(h) - \theta_r}{\theta_s - \theta_r}, \quad (6)$$

substituting Equation (5) into Equation (6), the $S_e(h)$ can be described by the vG parameters:

$$S_e\,(h) = \left(\frac{1}{1 + |\alpha h|^n}\right)^m. \quad (7)$$

Since Andosols present strong aggregation, which normally induces bi- or multi-modal SWR functions (Dörner et al., 2015), we included the bimodal (or dual-porosity) function for heterogeneous pore systems defined by Durner (1994). The equation is constructed by a linear superposition of effective saturation sub-curves as follows (Equation 8):

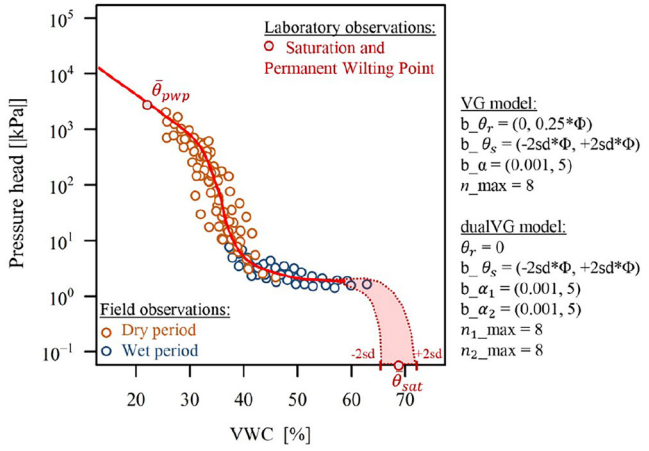

FIGURE 2 Graphical scheme: Fitting water retention functions using unsatfit. Boundaries for θ_s, θ_r, and α are denoted by the prefix "b_". The water content at saturation represents the total porosity (Φ).

$$S_e = \sum_{i=1}^{k} w_i \left[\frac{1}{1 + |\alpha_i h|^{n_i}} \right]^{m_i}, \quad (8)$$

where k is the number of sub-functions that form the total pore-size distribution and w_i are the weighting factors for the sub-curves, subject to $0 < w_i < 1$ and $\sum w_i = 1$.

The Python library "*unsatfit*" developed by Seki et al. (2022) was used to determine and optimize the hydraulic parameters. This package includes the program "SWRC Fit," which performs a nonlinear fitting of soil water retention curves by a Levenberg–Maquardt optimization method (Marquardt, 1963). A more detailed evaluation of this general model for multimodal unsaturated soil hydraulic properties is provided by Seki et al. (2023). As reaching total saturation at field conditions is not possible in a constantly draining system, the values of water content at saturation (θ_s) were fitted and constrained using confidence intervals of laboratory observations as boundaries. The laboratory determinations of θ_s ($n = 7$ per treatment) presented a Gaussian distribution (not shown). Therefore, the θ_s boundaries were considered a range of ±2 standard deviation from the mean value (Figure 2) to consider 95% of the probability distribution. Additionally, the laboratory determinations of θ_{PWP} were included during the fitting of all data sets to provide information on the driest extreme.

Regarding the vG parameters optimization, the maximum value for the n parameter was prescribed to 8 (Hohenbrink et al., 2023; Seki et al., 2022). The minimum and maximum boundaries of the α [kPa^{-1}] parameter were set as b_α = (0.001, 5) following Hohenbrink et al. (2023). This range for α provoked numerical instabilities that interrupted convergency during the iterative optimization of specific cases. This was encountered a few times when applied to too complex field SWR behaviors and the large number of observations. To overcome this during the iterative process, two error exemptions were included to try achieving convergence: (i) the maximum boundary of α was incremented by imposing b_α = (0.001, 20) for both subfunctions, and if this was not useful, (ii) bounds of b_α_2 and b_n were made free. These exemptions were useful to identify unreliable outliers in the analysis. Based on Hohenbrink et al. (2023), the boundaries for θ_r in unimodal functions were set to b_θ_r = (0, 0.25*Φ), being the total porosity (Φ) the mean values determined from our laboratory experiments. For bimodal functions, θ_r is prescribed to 0 by default.

2.5.2 | Statistical analysis

We analyzed the laboratory determinations for the complete profile. Nevertheless, since compaction effects were reported within the first 20 cm in the field (Dörner et al., 2023, 2022) and the highest temporal variability occurs toward the soil surface, the statistical analysis for continuous field observations was focused on 10- and 20-cm depths only. After applying the Shapiro–Wilk normality test, Levene's test for homogeneity of variance was conducted when residuals met the normality assumption. In such cases, the analysis of variance (ANOVA) was performed to identify differences between hydraulic parameters obtained from different soil water and structure dynamics. The test included all factors: treatment (T0, T1, and T2), sub-treatments (Station 1 and Station 2), depths (10, 20, and 60 cm, accordingly), periods (WP and DP), and cycles (wetting and drying). When data were not normally distributed, the Kruskal–Wallis test was performed over the multiple independent groups. To discern differences between two independent groups, the Mann–Whitney U test was automatically executed, facilitating pairwise comparisons. All statistical analyses, data processing, and plotting were performed in RStudio 2024.04.1+748 (Posit team, 2023) and corresponding libraries. The model performance was assessed by the Coefficient of Determination (R^2), the Root Mean Squared Error (RMSE), and the Akaike Information Criterion (AIC). The summaries and statistical results are presented in the Supporting Information.

3 | RESULTS

3.1 | Soil water dynamics in a volcanic ash-derived soil

The amplitude of soil water dynamic varies from upper to deeper layers. The VWC show higher variation close to the soil surface due to higher exposure to atmospheric conditions. In Figure 3, larger boxes and longer whiskers denote more variability in the amplitude of data oscillation at 10-cm depth for all treatments. No outliers were depicted beyond the whiskers range after the smoothing routine. Despite the

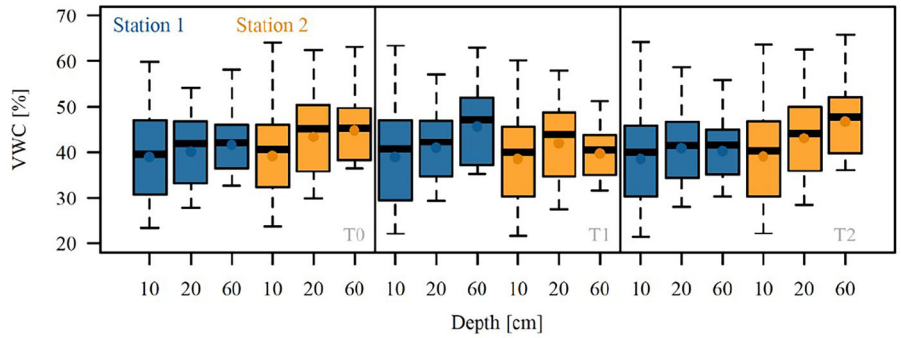

FIGURE 3 Boxplot of volumetric water content [VWC, %] time series at three depths (10, 20, and 60 cm) at each monitoring station. Additional colored dots describe mean values.

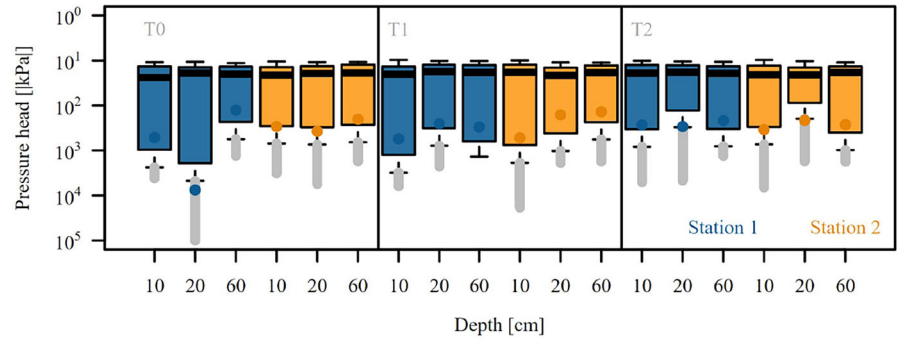

FIGURE 4 Boxplot of pressure head [|kPa|] time series at three depths (10, 20, and 60 cm) at each monitoring station. Additional colored dots describe mean values. Extreme values are presented by gray dots.

decreased variation toward deeper layers, mean and median values remain similar throughout the soil profiles. Mean VWC values ranged between 38.5% and 39.1% at 10 cm, 40.0%–43.9% at 20 cm, and 39.6%–46.7% at 60 cm (Table S1) including all stations.

In terms of pressure head, Figure 4 describes highly variable dynamics, where no clear trends can be observed. The median is similar at all monitoring stations and depths, ranging between −17.7 and −23.9 kPa. The mean values are strongly affected by extreme pressure heads that vary up to three orders of magnitude. Particularly, T0-station 1 at 20 cm described highly negative values that reach up to −99,999 kPa. In this individual case, observations are not reliable and considered artifacts, probably produced by soil shrinking/cracking and the subsequent detachment of the sensor ceramic disk from the soil during extreme dryness. Considering the time series full length, the range of pressure head observations represented by the second and third quartiles varied approximately between −12 and −1200 kPa (Table S2).

Both VWC and pressure head time series describe the large storage capacity and high median pressure head of these soils, representing a generally wet status under the humid-temperate conditions. Additionally, time series data show that these soils hold high water contents at very strong matric suction (i.e., VWC > 20% at ≈−1000 kPa) at the three described depths.

3.2 | Soil water content bimodal distribution into wet and dry periods

Figure 5 presents histograms (gray bars) of VWC time series from each station (Stations 1 and 2) at each compaction treatment (T0, T1, and T2). In addition, the pdf is computed and presented. As expected, the red-solid line pdf calculated from the total number of observations (N = 105,121) describes a bimodal distribution with two main peaks: a high relative frequency of observations at the left-hand side (between ≈22% and 55%), which represents the dry period dynamics (DP; peak at VWC ≈25%), and a high relative frequency at the right-hand side (between ≈39% and 62%), corresponding to the wet period dynamics (WP; peak at VWC ≈47%). To represent each WP (blue-dashed line) and DP (orange-dashed line) observations, the figure includes the resultant proportion of the pdf for each period. The area under the curve is colored accordingly. Implementing the θ_μ to separate wet and dry conditions allowed for obtaining Gaussian-shaped

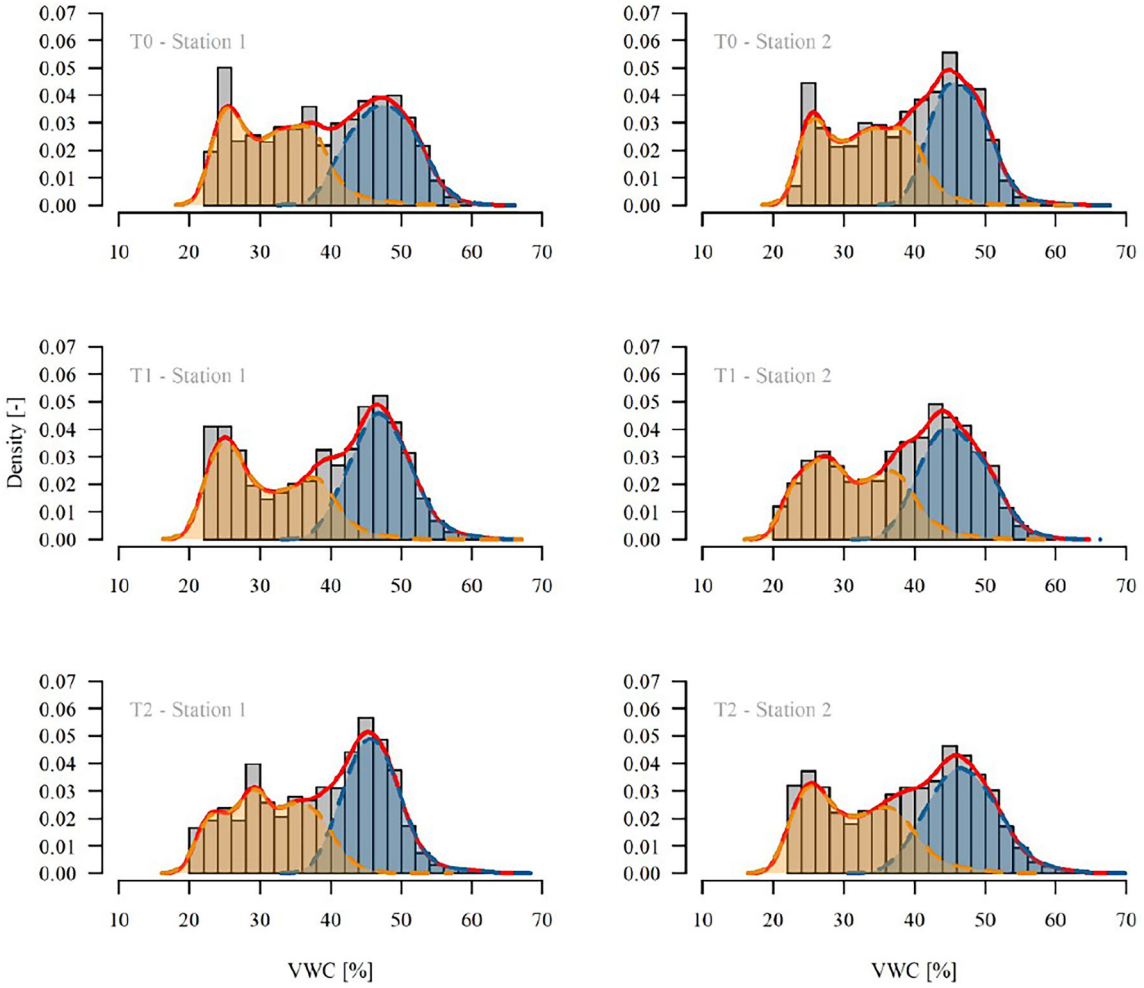

FIGURE 5 Histogram (gray bars) and probability density function (pdf) of the total number observations per time series (red line). Blue and orange lines represent the separated distributions for WP and DP, respectively.

distributions in the case of WP dynamics. Regarding DP dynamics, the distribution does not have a Gaussian shape. This distribution contains a third smaller and smoother peak that overlaps the WP distribution (at ≈36%). This third small distribution represents important wetting and drying processes in the dry season, as well as VWC observations in the slow transition from wetter to drier conditions in spring.

3.3 | Soil water dynamics and pore-size distribution

In Figure 6, a VWC time series is presented as an example (a complete presentation of time series is included in Figure S2). When analyzing the VWC as a function of time, rapid responses to precipitation events can be discerned. When including information on the pore-size distributions obtained at laboratory conditions (colored background), an approximation to water-filled pore volumes as contrasted to the soil water dynamic is presented. The separation of observations into wet and dry period dynamics is included, where blue and orange segments describe WP and DP, respectively (Figure 6). WP soil water dynamics generally occur through a larger radii porosity, while most of medium (MP) and fine (FP) pores are filled with water. Therefore, rapid variations of VWC would be mainly affected by the properties of macropores (MaP), narrow (nCP), and wide (wCP) coarse pores. During WPs, the dynamics exhibit a higher frequency and less amplitude, since the range of variation is constrained to the remaining empty space between a large volume of water-filled pores and the saturation point (0 kPa; θ_s). Therefore, it results in high variability with lower magnitude changes. On the other hand, DP soil water dynamics mainly occur in the medium pores (MP) range, where VWC changes face higher retention forces. Nevertheless, it is expected that new inflows were distributed through larger pores such us nCP, where peaks of VWC increments are rapidly dissipated due to high hydraulic conductivity in the infiltration/drainage process. During DPs, the range of VWC variation is larger because of a greater volume of empty pores. Thus, the soil water dynamics describe a larger amplitude and a lower variability due to less precipitation events.

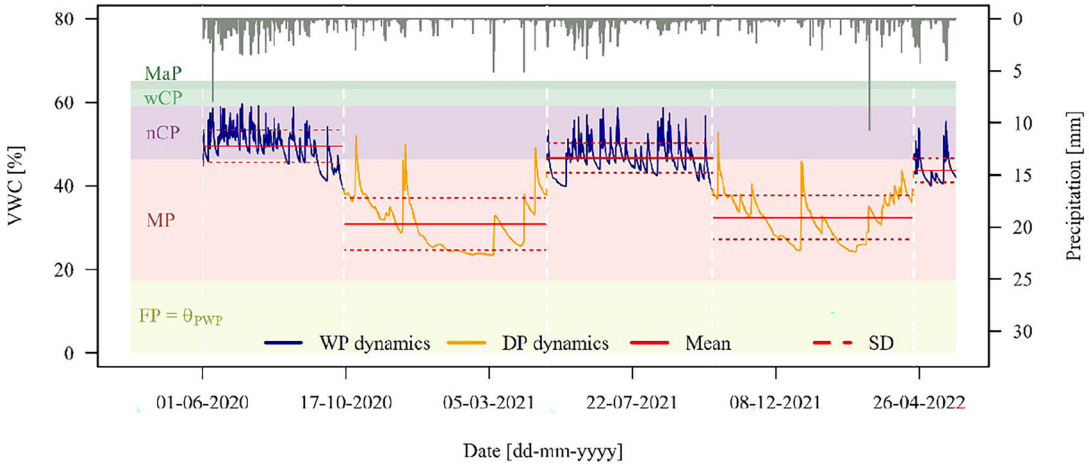

FIGURE 6 Volumetric water content (VWC; %) corresponding to T0, Station 1, at 10-cm depth, as an example, with colored segments for wet (WP, dark blue) and dry (DP, orange) period dynamics separation. Each period presents the mean VWC (red solid line) and the respective standard deviation (red dashed line). The colored background areas delineate the VWC range for the pore-size distribution classes determined at laboratory conditions. The volume of FP corresponds to the permanent wilting point (θ_{PWP}), and the summation of all classes to the saturation water content (θ_s). Gray bars represent precipitation (mm). Data temporal resolution is 10 min. FP, fine pores; MP, medium pores; MaP, macropores; nCP, narrow coarse pores; wCP, wide coarse pores.

3.4 | Laboratory-based soil water retention functions

Since we focus on the influence of soil structure dynamics on hydraulic properties represented by SWR models, for a detailed description regarding short-term impacts of the compaction treatments on soil mechanical properties and pore functionality, we refer to Dörner et al. (2022, 2023). In short, the experimental field described (i) a reduction of macropores volumes and air conductivity leading to critical values of air capacity, (ii) differences in penetration resistance that dissipated by equilibrating to external stresses due to animal trampling and wetting/drying cycles, and (iii) a limited effect on soil precompression stress and plant available water.

Figure 7 depicts the SWRCs obtained in laboratory conditions and the fitting of both unimodal and bimodal formulations of the van Genuchten equation. In general, no significant differences between unimodal and bimodal fits were detected (Table S3). The characteristic multimodal shape of the SWRC of Andosols was smoothed when averaging soil sample replicates ($n = 7$). In some cases, such as T0 at 10-cm depth (e.g., Figure 7, left column, top-row), the bimodal SWRCs captured a pronounced inflection point between −6 and −33 kPa. In this case, the bimodal curves also erratically deviated over more negative matric potentials. This is produced by an incipient secondary inflection point around −15 to −33 kPa and the lack of observations toward −1543 kPa in the available laboratory approach. In other cases, such as T0 and T1 at 60 cm (Figure 7, left and middle column, bottom row, respectively), the bimodal formulation is able to represent the curvature between −3 and −33 kPa, describing a marked change in the properties from structural to textural porosity. Data points describe remarkable inflection points occurring at −6 and −15 kPa at all depths and treatments, which suggest a hierarchy between three groups: (i) macroporosity (MaP) and wide-coarse pores (wCP), (ii) narrow-coarse pores (nCP), and (iii) MP to FP. When considering 60-cm depth, the FP volume increases to around 30%.

In all other treatments and depths, the unimodal van Genuchten numerical solution did not differ substantially from its bimodal form, both yielding high-fitting performance ($R^2 > 0.96$ and RMSE < 2.42 kPa for unimodal, and $R^2 > 0.99$ and RMSE < 1.39 kPa for bimodal). Additionally, the Akaike information criterion (AIC) values were slightly lower for the bimodal formulation, generally for T0. The unimodal function presented lower AIC in T1 and T2 at 10- and 20-cm depth (Table S3). Considering a balance between the R^2 and AIC values, the unimodal function meets the expectations of being the best representation for laboratory determinations. The parameters of this function presented statistical differences. θ_s and α increased toward deeper layers, describing strong statistical differences at 60-cm depth (p-value < 0.001). The n parameter only showed differences between 10- and 60-cm depth, being lower at the deepest layer. θ_r was statistically higher (p-value < 0.01) at 60-cm than 10- and 20-cm depth (Table S4). The bimodal function described similar statistical differences for θ_s. Regarding other parameters, no differences were found other than α_1 being statistically lower in 60 than 20-cm depth (Table S5). No statistical differences in SWR parameters for both functions were found between compaction treatments using laboratory samples.

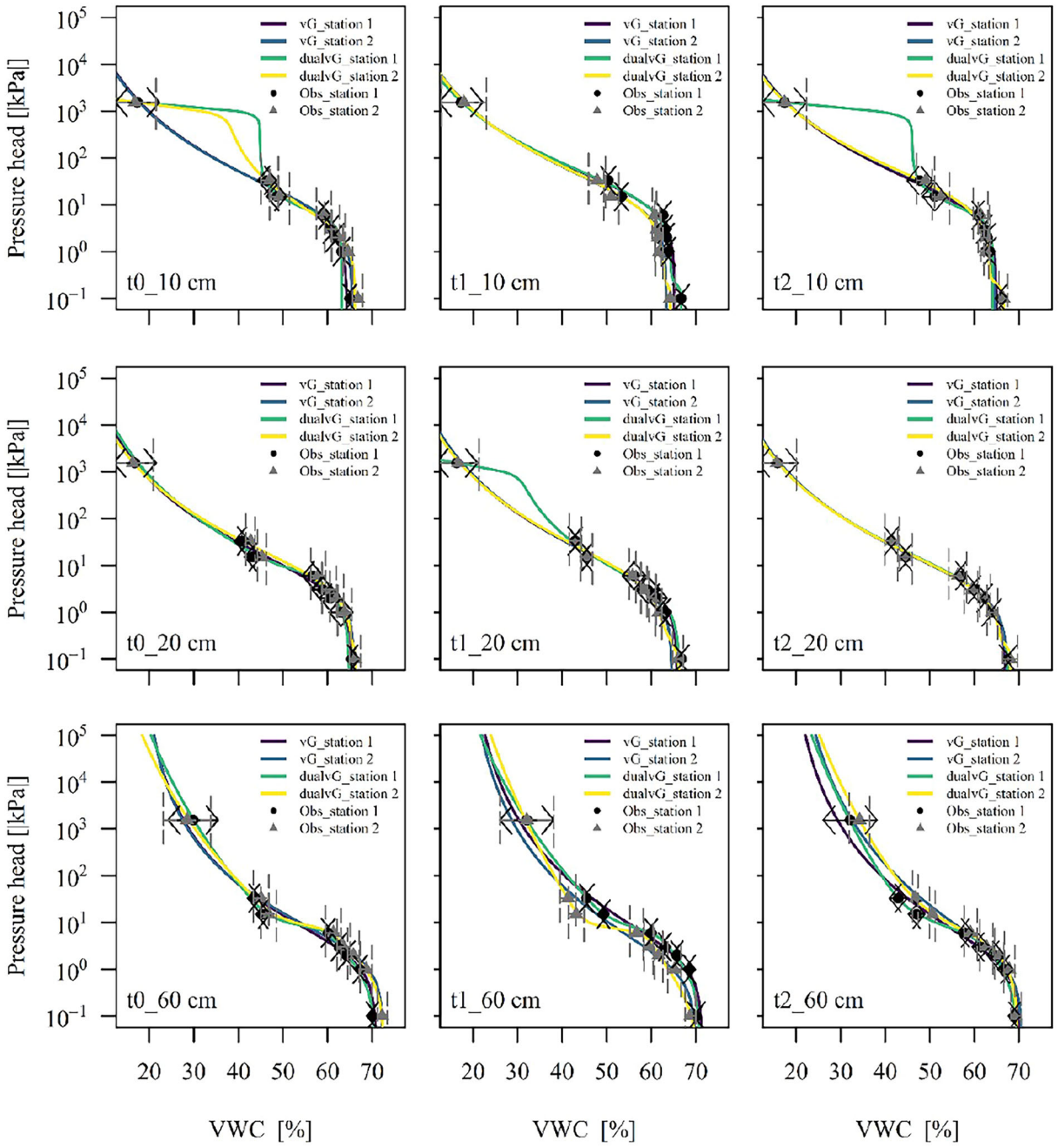

FIGURE 7 Unimodal (vG) and bimodal (dualvG) van Genuchten models fitted (lines) to laboratory water retention observations (symbols) at three depths (rows) for stations 1 (solid black circles) and 2 (solid gray triangles) at each compaction treatment. Left, middle, and right columns correspond to T0, T1, and T2, respectively. Straight-head and arrow-head error bars are included for station 1 and 2 measurements respectively.

3.5 | Dynamic soil water retention functions at field conditions

3.5.1 | Influence of wetting/drying cycles and compaction treatments

Figures 8 and 9 describe bimodal SWRCs considering wetting and drying cycles in the two upper layers of each compaction treatment. The fitted parameters area are visualized in Figures S4 and S5. The model's performance was very high ($0.91 \leq R^2 \leq 0.97$) excepting when fitted to drying cycle observations in T1, Station 1, at 20-cm depth ($R^2 = 0.67$). The RMSE varied from 0.92 to 2.90 kPa, being generally higher when fitting to drying cycles (Table S6).

There were no statistical differences in the parameters when including wetting and drying cycles (Table S7). The mean θ_s predicted by the models is 67.7%. The weighing factor (ω) is about 0.44, which describes a relatively balanced contribution from both subfunctions representing structural and textural pore volumes. The first subfunction described lower values

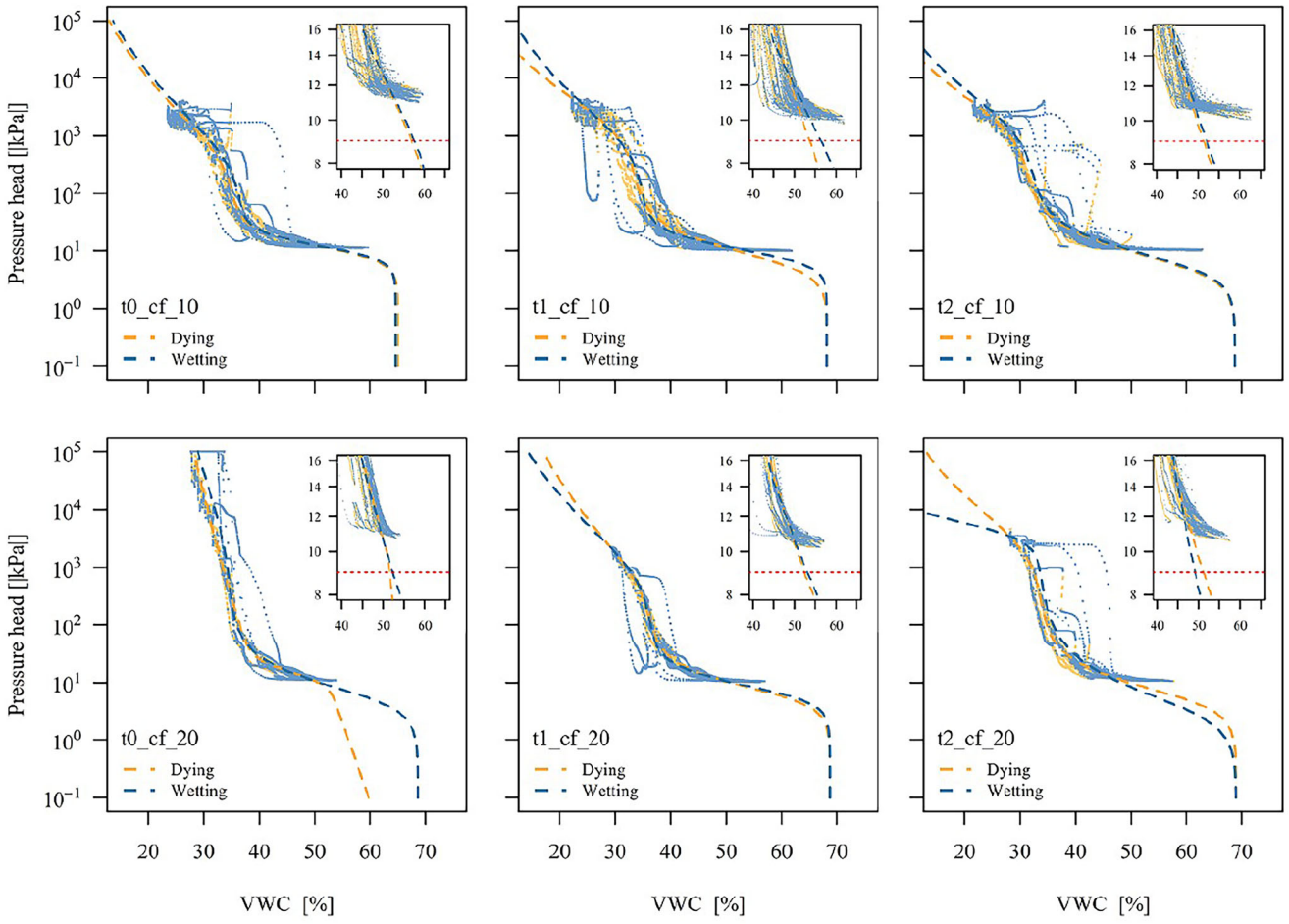

FIGURE 8 Bimodal van Genuchten model (dashed-lines) fitted to wetting (light-blue) and drying (orange) cycles data for station 1 at each compaction treatment. The horizontal red dashed-line in the zoomed-in plots describes the absolute value of the sensor-s air-entry potential (−9 kPa).

for the parameter α and higher for n, being the mean values of α_1, α_2, n_1, and n_2 around 0.11 kPa^{-1}, 0.45 kPa^{-1}, 3.3, and 1.2, respectively (Figure S3). Compaction treatment showed statistical differences (Figure S4). The θ_s parameter was statistically higher in T2 (p-value < 0.01). The α_1 parameter was significantly lower at T0 (p-value < 0.01). Regarding the second subfunction, α_2 was statistically lower in T1. In T0 at 20 cm, the α_2 parameter was fitted at the upper bound ($\alpha_2 = 5$ kPa^{-1}), which probably influenced the statistical differences respect to T1 (Figure S4).

Focusing on the SWRCs, Figures 8 and 9 show the good performance of the bimodal (or dual-porosity) model to describe important inflection points observed in field data. Important hysteretic loops are described, which suggest the influence of strong hydraulic non-equilibrium. The observations over these loops (or scanning curves) did not influence the fitting of bimodal wetting curves, which parameters did not statistically differ from the drying curves. An important amount of scanning curves follows a non-systematic behavior, showing faster changes of VWC followed by a delayed re-equilibration of the pressure head. These loops are not hysteretic behaviors. Instead, they may be produced by the asynchrony of sensors readings when reacting to a wetting front. This suggests that heterogenous water flows may be reaching moisture sensors faster than matric potential sensors. Figure 8, bottom plots the left and right column, describes some deviations in the model fitting at the extremes of the function, when drying and wetting curves misfit toward the wet and dry ends, respectively. Further analysis is required since this does not happen in Station 2 under similar conditions of data availability.

The top-right zoomed-in plots presented for each condition in Figures 8 and 9 describe SWR observations at the wettest ranges observed at field conditions. A clear inflection point is found between −10 and −14 kPa. Nevertheless, neither wetting nor drying fitted curves were able to represent this curvature.

3.5.2 | Influence of soil moisture states and wetting/drying cycles on dynamic SWR parameters

Figures 9 and 10 show SWRCs derived by bimodal functions for wetting and drying cycles at each compaction treatment for WP and DP dynamics. WP and DP dynamics showed

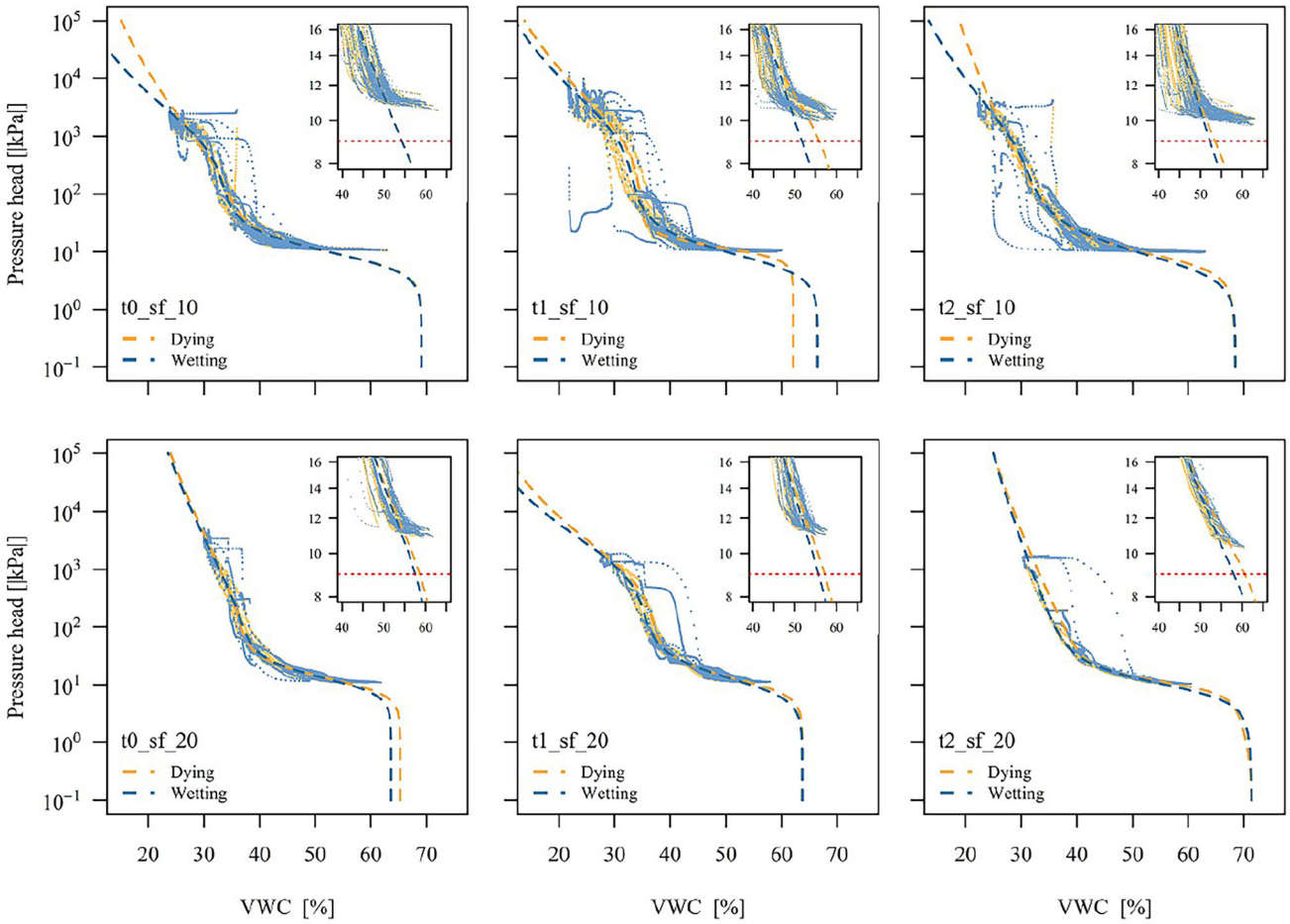

FIGURE 9 Bimodal van Genuchten model (dashed-lines) fitted to wetting (light-blue) and drying (orange) cycles data for station 2 at each compaction treatment. The horizontal red dashed-line in the zoomed-in plots describes the absolute value of the sensor-s air-entry potential (−9 kPa).

statistical differences in all parameters of the first subfunction (α_1 and n_1), as well as in the weighing factor w. Due to the possible impact of the data availability on the parameters of dual-porosity model subfunctions, we focus on describing this effect from a model fitting perspective, rather than seeking for physical meaning. Conversely, statistical focus was placed on comparing wetting and drying cycles within these periods.The fitting performance was moderate to very high for both WP and DP. The WP-R^2 values ranged from 0.60 to 0.97 with a mean of 0.77, and the DP-R^2 values varied from 0.69 to 0.95 with a mean of 0.85. The RMSE varied from 0.78 to 2.73 kPa for WP and from 0.76 to 4.06 kPa for DP. The overall averaged RMSE values were 1.79 and 1.92 kPa for WP and DP, respectively (Table S8).

The visual overview of the two subfunctions parameters is presented in Figure S5. Regarding WP dynamics, the parameters of the first subfunction described smaller values than in DP. The α_1 parameter shows concentrated values with a mean of 0.097 and 0.096 kPa^{-1} for drying and wetting cycles, respectively. The n_1 parameter showed larger and more scattered values during WP than DP dynamics, being the mean around 7.1 (close to its upper bound). In the case of DP, the mean n_1 was slightly higher but not significant during wetting ($n_1 = 3.2$) than drying ($n_1 = 2.6$). Interestingly, the w factor is lower, but similarly, scattered during WP than DP, being the mean around 0.25 and 0.48, respectively. In the second subfunction, only α_2 showed clear differences, showing smaller values during DP (<0.1 kPa^{-1}) than WP. Some outliers with large values influenced the mean of WP. The n_2 parameters did not change due to fitting over WP and DP dynamics and varied between 1.23 and 1.28. The detailed statistical results are presented in Table S9.

In Figures 10 and 11, wetting and drying observations are presented along with the fitted curves obtained using the bimodal van Genuchten model for Station 1 and Station 2, respectively. In these figures, observations and fitted curves are separated by compaction treatments, depths, periods, and cycles.

Based on the field observations behavior, SWR data vary not only between compaction treatments and soil depths, but also when considering contrasting soil water dynamics during WP and DP, as well as wetting and drying cycles. The pattern

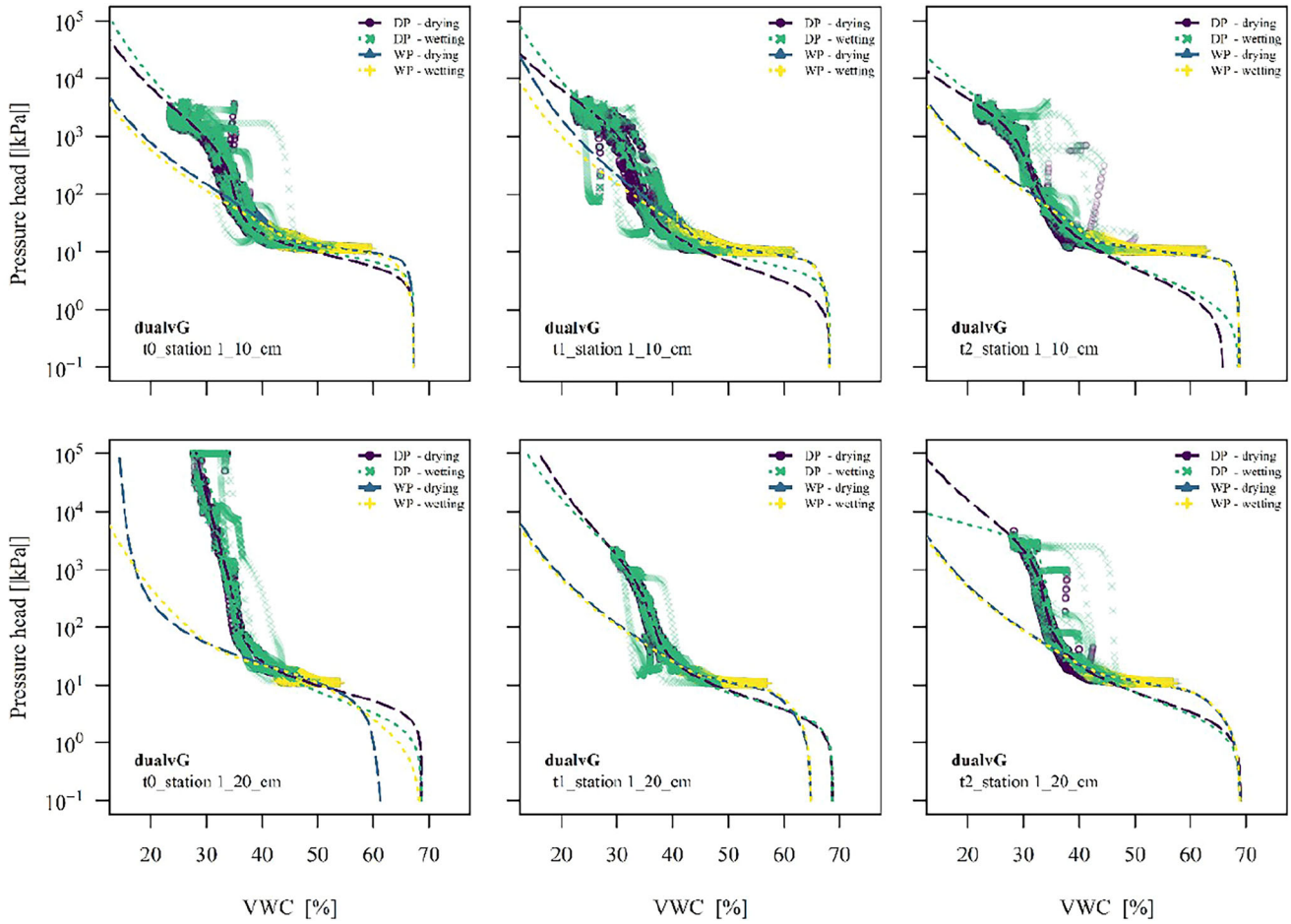

FIGURE 10 Bimodal van Genuchten model (dualvG) fitted (dashed-lines) to wet (WP) and (DP) periods considering wetting and drying cycles observations (symbols) for station 1 at each compaction treatment. Left, middle, and right columns correspond to T0, T1, and T2, respectively.

of spatiotemporal variability is similar in both Station 1 and Station 2 within each compaction treatment. Different scanning curves described strong hysteresis toward the surface, which decreased in the most compacted soil.

Differentiating SWR data in WP and DP dynamics provide additional insight to understand the spatiotemporal variability of SWR properties. Wetting and drying cycles during WP dynamics described a more homogenized behavior. The large volume of water-filled pores constrains the new inflows and outflows to short quick flows through the structural porosity. The variability of soil water retention dynamics increases in DP dynamics. For this last condition, the figures describe a range of scanning curves during wetting and drying cycles creating a cloud of points. Particularly, extreme hysteretic behaviors relate to wetting cycles. The deviation of wetting cycles during DP dynamics is remarkable since it might reflect complex interactions between variably connected pore networks occurring even above 30% VWC. When considering the increase in compaction from T1 to T2, the cloud of observations is narrower and presents more defined hysteresis loops. This could be related to the collapse of the soil structure, decreasing the diversity of pore-networks and their inter-connectivity.

Extreme wetting loops occurred during DP at different depths. These loops described different rates of change and followed clear pathways. In most of these cases, a fast change in pressure head follows a slow increase of VWC. This expected relation is in accordance with Vogel et al. (2023) and Hannes et al. (2016) and particularly assumes that both changes start at the same time with different rates of change. Therefore, these extreme loops suggest fast and more simultaneous readings of the water inflows by both VWC and pressure head sensors. Conversely, non-systematic behavior is also described during wetting cycles during DP dynamics at all depths (Figure S6). Even though our 1D analysis averaged the three VWC measurement replicates per depth at each time step, this shows that the persistent mismatch in time happens during drier conditions and over a wide range of water contents (up to ≈35% VWC). This phenomenon is certainly enhanced when considering individual sensor observations due to their different amplitude of variation (results not shown).

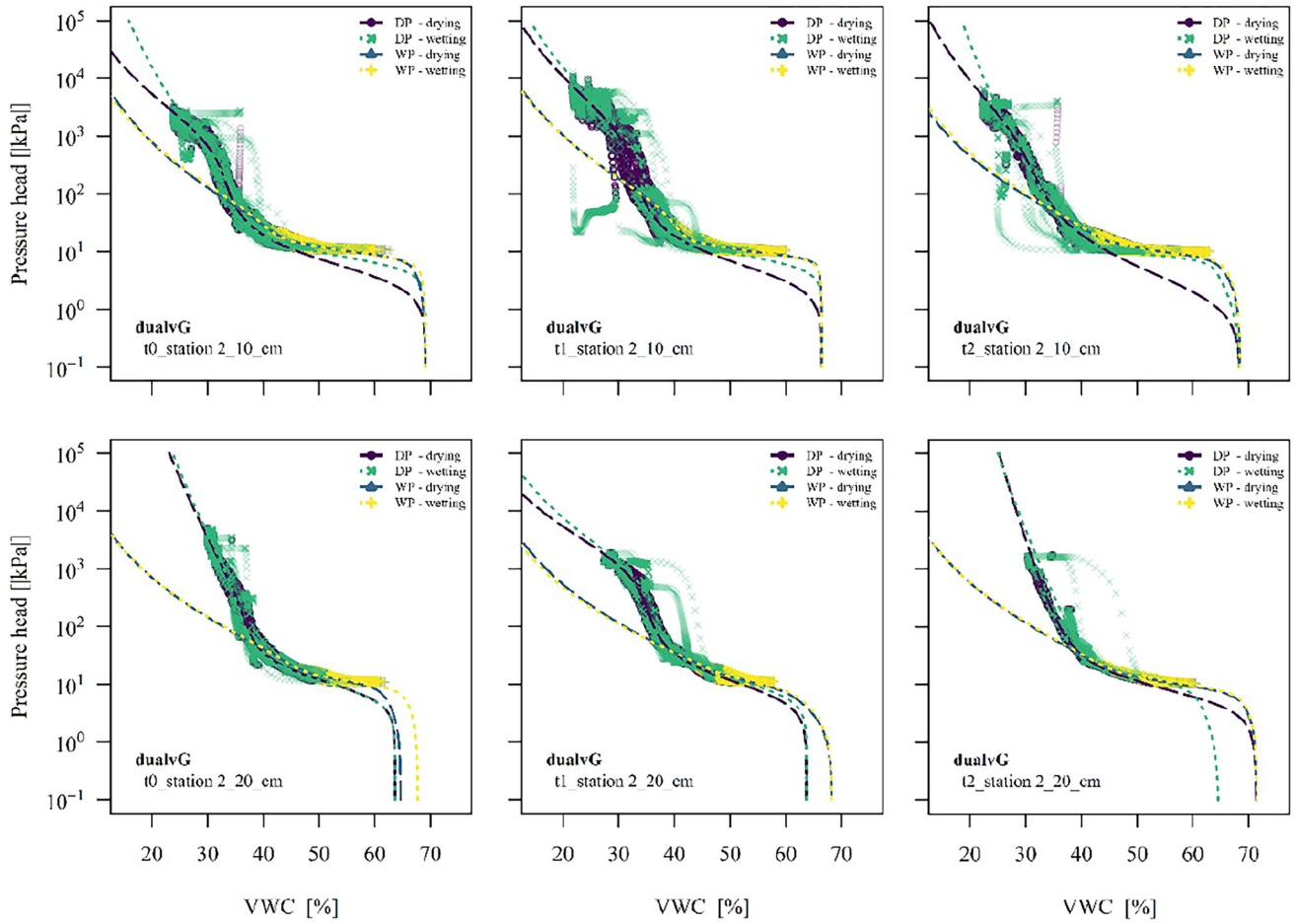

FIGURE 11 Bimodal van Genuchten model (dualvG) fitted (dashed-lines) to wet (WP) and (DP) periods considering wetting and drying cycles observations (symbols) for station 2 at each compaction treatment. Left, middle, and right columns correspond to T0, T1, and T2, respectively.

Focusing on the modelled curves, the number of observations at different ranges of the SWRC influences the definition of complex curvatures during the optimization process. Strong curvature shaped by the observations is well described in all fitted SWRCs, producing complex inflection points and better approximating the wetter extreme of the observations. The availability of observations, by means of both the covered range and number of points, has an important influence on the resulting curves. The relationship between the highest water contents observed in the field, along with the probability range of water content at saturation determined under laboratory conditions, influences the shape of the curves near saturation (approximately from −10 to 0 kPa). When fitting this function to the total range including WP and DP together (Figure S7), it is still not able to represent the strong curvature around field capacity, which affects the description of the wCP and predicted MaP ranges. A very good fit to the wetter extreme of the observations is obtained by using WP observations only.

4 | DISCUSSION

4.1 | Combining data to obtain SWRCs: Aligning process and observation scales

Representing soil water dynamics not only depends on the parameterization of the soil hydrological properties (N. Jarvis et al., 2016) or the implemented model (Šimůnek et al., 2003), but also on the characteristics of the observations used to inform them. Sometimes, the required observation scale might not align with the targeted process scale. Whether prioritizing the spatial or temporal resolution, it is important to reflect on the interpretability of measurements in terms of the scale attributes. These attributes are the extent, the spacing, and the integration volume for the space domain, and duration and resolution for the time domain (Blöschl & Sivapalan, 1995). This framework guides our analysis on the spatiotemporal variability of flow phenomena due to soil structure dynamics.

Regardless of the multimodal nature of SWRCs of Andosols and lower AIC values resulting from the bimodal formulation, the unimodal van Genuchten function seems to be the sensible choice for the Pedon scale from laboratory observations. This can be related to the lack of SWR points at different pressure heads and the decrease in curvature due to approximating this function to averaged observations (Figure 7). Despite this, the bimodal function might be required when soil structure in Andosols has developed for longer times. Studies conducted in southern Chile described remarkably complex SWRCs (Dörner et al., 2010, 2015).

Based on the space scale attributes of our laboratory samples, the observations described a core-to-Pedon scale. Our results not only showed common characteristics of the soil water retention in volcanic soils (Bravo et al., 2020; Dörner et al., 2015; Mosquera et al., 2021), but also followed the general trends found when comparing laboratory and field determinations (Basile et al., 2003; Huang et al., 2021; Mosquera et al., 2021; Pečan et al., 2023; Zhang et al., 2017). The characteristics of SWRCs in soil cores allow us to visualize a well-structured soil with defined inter and intra aggregates porosity. This is normally described for volcanic soils in a wide range of conditions and land uses (Dec et al., 2017; Dörner et al., 2010, 2015; Seguel & Horn, 2006). The observed structure suggests several pore networks providing (i) fast-flow drainage channels (MaP and wCP), (ii) two domains within the nCP range providing slow-flow drainage (−6 to −15 kPa) and easily available water (−15 to −33 kPa), and finally, (iii) available water pores in the MP range. With such characteristics, these soils are prone to PF, which has been visualized through field dye-tracer experiments in southern Chile (Blume et al., 2008, 2009) and could be enhanced by the applied compaction (Kulli et al., 2003).

Generally, the conditions provoking heterogeneous infiltration fronts (or PFs) are mainly subscribed to drier conditions in soil, where nonequilibrium states, crack formation, and the increased water repellency are strongly influential (N. Jarvis et al., 2016; Nimmo, 2021; Ritsema et al., 2005). These factors have been documented in southern Chile's Andosols during the drier conditions (Blume et al., 2009; Dec et al., 2017; Ellies et al., 2005). Nevertheless, Andosols still hold large water contents at drier states. The VWC at the permanent wilting point (1543 kPa) normally ranges between 20% and 30% in the first 60 cm (Bravo et al., 2020; Dec et al., 2022; Dörner et al., 2015), and our field observations showed water contents above 20% retained at ≈−1000 kPa. This can be related to the complex pore structure in volcanic ash soils, which presents high porosity and high clay contents and induces a sandy behavior near saturation and a large water holding capacity at low matric potentials (Dörner et al., 2010). This suggests further analysis to define the hydraulic processes of PFs as influenced by such extreme soil physical properties in order to understand the contribution of potential mechanisms, such as funneled flow, fingered flow, or macropore flow (Nimmo, 2021).

Laboratory measurements show the initial conditions of the soil compaction experiment (September 2019). Therefore, they represent a single structural state of the porous system at the time of sampling (Herbrich & Gerke, 2017). Since then, these plots have been exposed to both external (soil compaction events by sheep grazing) and internal (wetting and drying cycles) mechanical stresses. In this study site, Dörner et al. (2022) described that structural changes reduced the total porosity and increased the water retained in the soil due to (i) a reduction of both MaP and wCP and (ii) an increase of MP. Temporal dynamics of spatial variability in soil mechanical strength at the plot scale showed that compaction impacts remained located above 20-cm depth (Dörner et al., 2023). At the cylinder scale, a micro-penetrometer analysis showed the formation of platy structure at the surface of T2. These previous investigations over the study site described higher temporal dynamics than spatial variations within plots. Thus, we might assume that our analysis at the core-to-Pedon scale can approximate to the plot level.

We will now focus on the time scale attributes of our continuous field observations, which cover the Pedon scale. The used 10-min resolution allowed us to perceive variations at very small temporal scales and different relations of soil water retention. This described not only a diversity of possible scanning curves during wetting and drying cycles, but also the temporal mismatch constraining concomitant measurements.

The three replicates per depth averaged at each time step in the one-dimensional VWC profile allowed for the representation of temporal variability of infiltration fronts. Using mean values of VWC per time step produced a small effect on the magnitude of the resulting water content changes and conserved the fastest reaction time of the VWC replicates at each rainfall event. The resulting VWC temporal dynamic is compared with the single matric potential sensor at each depth. Similar reaction times exhibited by the VWC and pressure head observations at the same depth indicated a homogenized wetting front. This will describe a systematic behavior when visualizing the SWRCs (Hannes et al., 2016). On the contrary, asynchrony in the reading times between VWC and pressure head observations would then indicate a heterogeneous wetting front. Consequently, a non-systematic behavior is depicted as artifact, which is not part of the described hysteresis. The occurrence of asynchrony in sensors' readings poses uncertainty in data quality and risk to erroneously describe hysteresis in SWR functions. Nevertheless, the detection and careful interpretation of the processes behind non-systematic behaviors may provide alternatives to understanding the environmental factors influencing the temporal occurrence of non-uniform flows.

4.2 | Data quality and processing framing the interpretations

High-resolution sensors are prone to describe noise. Therefore, several routines have been developed to improve data quality (Hannes et al., 2015, 2016; Peters et al., 2014). In our research, a fundamental question is whether measuring fast enough represents the intra-Pedon spatial heterogeneity and its influence on the different sensors' reading time. In the optimal scenario, concomitant measurements of water content and matric potential not only refer to the same spatial location but also represent the same flow phenomena. To achieve this, researchers might aggregate observations to a certain temporal resolution so that wetting and drying cycles can be clearly identified (Hannes et al., 2016; Herbrich & Gerke, 2017). More commonly, the focus is constrained to main drying processes only, making sure that sensors' readings are simultaneously showing a soil water decrease (Huang et al., 2021; Pečan et al., 2023; Zhang et al., 2017). Generally, these approaches consider a one-dimensional profile with a single pair of sensors (θ, h) per depth.

As mentioned above, the influence of soil structure heterogeneity would result in non-uniform flows asynchronously arriving to the volume of influence of sensors, which should be reflected by non-systematic soil water retention variations. In our approach, after transforming our data from a 2D to 1D profile, averaging VWC replicates smoothed the local spatiotemporal heterogeneity per depth to a single VWC value at each timestep. These averaged values do not significantly influence the magnitude of the resultant water content. Temporal dynamics at small scales are affected. Nevertheless, this conserves the fastest reaction time from these sensors, which can still describe the asynchrony when related to the matric potential readings.

Hannes et al. (2016) analyzed water retention during wetting and drying cycles by implementing several hysteresis models over 3-year high-resolution data sets. To do so, they reduced the number of observations and conserved the main patterns by averaging every 3-hour periods and applying moving average routines. This smoothing routing was skipped during fast wetting peaks so that these dynamics could be preserved. Their water retention results described systematic behavior only. Therefore, they assumed simultaneous sensor readings within a macroscopically homogeneous soil. From this approach, the soil–water retention behaviors, or scanning curves, were classified into three categories that are important to interpret our findings: (i) the hydraulic nonequilibrium, as the redistribution phase behind drainage and imbibition occurring in terms of hours; (ii) the quasi-equilibrium hysteresis, as defined soil–water retention relations over the scale of weeks, and (iii) structural dynamics, which relate to soil structure development and seasonal behaviors occurring in terms of years.

Visually, our results describe the three abovementioned behaviors. These are clearer at 10 cm due to more variable soil water dynamics. Interestingly, nonequilibrium relations are easily recognizable in the more compacted treatments, while the hysteresis between wetting and drying cycles of quasi-equilibrium and structural dynamics curves decreases. This might describe the collapse of a diversity of interconnections within the structural porosity (MaP and wCP) due to compaction. This aligns with previous soil physical and mechanical assessments in the study site (Dörner et al., 2022). The remaining pore networks seemed to promote extreme differences in less diverse SWR behaviors.

4.3 | The influence of heterogeneous flows on parameters

The soil structure heterogeneity allows a range of possible flow variations. As it interacts with environmental dynamics, these possibilities are temporally visible through the activation of different pore networks that shape the occurring wetting front. This temporal variability was described by the field observations but could not be represented using single SWRCs, particularly in our case, by a pseudo-hysteresis approach fitting to wetting and drying curves separately. Through this dynamic interplay, we might define peaks of spatiotemporal homogeneity or heterogeneity, which are dependent on the studied scale and could be depicted by looking at WP and DP dynamics. The temporal variation of the soil moisture spatial variability in a catchment scale exhibits peaks of homogeneity during either very dry or very wet conditions (Rosenbaum et al., 2012). At the pore-to-Pedon scale, the spatial variability of soil water content is generally higher under drier conditions, promoted by high rainfall intensities (van Schaik et al., 2008) and making PFs clearly visible (Blume et al., 2009; van Schaik et al., 2010). As observed in our results, the soil compaction impacts on the pore configuration and its structural dynamics moderate the extent of the temporal variability of SWR field behaviors.

The smaller range of SWR variation during WP describes homogeneous wetting and drying cycles. The soil maintained a moisture status around field capacity (mean $h \approx -15$ kPa at all depths), and this condition played a key role as a homogenizing factor since water interconnected a diversity of pore networks. This temporal homogenization of the soil system response was identified using cross wavelet analysis on soil water state variables and temperature dynamics (Bravo et al., 2020). The derived van Genuchten parameters showed no differences between wetting and drying processes during WP. Nevertheless, the representation over the wetter range of our observations (and the inflection point between −10 and −14 kPa) was improved when considering WP data only. This can improve hydrological models performance when using

matric potential sensors that are not able to cover the near saturation range. Small changes in the near saturation range importantly affect the variability of predicted saturated flows (Vogel et al., 2000).

The spatial heterogeneity in the soil water distribution increases during DP dynamics. The van Genuchten parameters did not show statistical differences during wetting and drying cycles since we constrained ourselves to fit one single curve per dynamic only, even though extreme hysteretic loops were evident. The bimodal van Genuchten formulation described important inflection points. The field observations showed that drying processes at DP are more homogeneous than wetting processes and relate to quasi-equilibrium states or structural dynamics. On the other hand, nonequilibrium scanning curves are described by wetting processes in DP only, which were enhanced in more compacted treatments. Therefore, the peak of heterogeneity can be identified from these dynamics.

Representing the spatiotemporal variability in the unsaturated zone using accessible and extensively used tools as equilibrium-based models is challenging. Implementing a pseudo-hysteresis fitting approach to describe continuous temporal dynamics of field SWR observations was not feasible at all, even though the models' fit described a very high performance. When factor time is included to predict SWR observations during wetting and drying cycles, the model performance varies considerably due to the encountered peaks of homogeneity or heterogeneity in soil water dynamics. Further research needs to be performed to explore what insights non-systematic behaviors hold, and whether considering them would be a proxy to predict the environmental conditions that trigger non-uniform flows in a simple and affordable way. Especially, emphasis should be placed on finding trends on how soil structure dynamics shape the soil hydraulic properties variability, not only as a result of the intrinsic soil pore rigidity and its relation to agricultural management (Huang et al., 2021; Pečan et al., 2023), but also due to the temporal evolution through soil structure formation or soil physical degradation (Dörner et al., 2023, 2022).

5 | CONCLUSION

Changes in soil structural dynamics, along with the spatiotemporal variations of soil water flows during contrasting moisture conditions, shape the intensity of soil water retention variability derived from continuous field observations, complicating soil water retention model fits

Combining scale attributes of spatial and temporal observation can help us align measurements with the targeted process scale, allowing us to discern hysteretic soil water retention from non-systematic behaviors produced by non-uniform flows.

The characteristics of laboratory observations, in our case representing the core-to-Pedon scales, may not always match field dynamics and require careful interpretation. In this study, the heterogeneous soil pore structure of an Andosol suggested the presence of non-uniform flows. The extrapolation of these behaviors across core-Pedon-plot scales can be accomplished by the spatiotemporal assessments of soil structural dynamics.

We emphasize the key role of data quality and processing in framing our interpretations as well as the sensitivity of high-resolution field monitoring sensors to temporal dynamics of soil water flows, which impacts the estimation of soil hydraulic properties. Despite the variability in soil water retention observations during wetting and drying cycles, a commonly used equilibrium-based approach applied in a pseudo-hysteresis form was not able to describe statistical differences in the van Genuchten parameters.

The interplay of soil structure dynamics and environmental conditions determined the intensity of hysteresis in soil water retention. Soil physical degradation due to compaction decreased the diversity of scanning curves. Therefore, soil structure and its dynamics are important in defining the boundaries of soil hydraulic properties variability. Along with the soil structural characteristics, contrasting conditions of soil water states in wet and dry periods help to disentangle the spatiotemporal variability of soil hydraulic properties. This dynamic-based approach allows us to identify peaks of homogeneity or heterogeneity that could contribute to a better representation of soil water phenomena across scales.

AUTHOR CONTRIBUTIONS

Sebastián Bravo Peña: Conceptualization; data curation; formal analysis; investigation; methodology; software; validation; visualization; writing—original draft. **Loes van Schaik**: Supervision; validation; writing—review and editing. **Jose Dorner**: Investigation; methodology; project administration; resources; validation; writing—review and editing. **Jos C. Van Dam**: Supervision; validation; writing—review and editing.

ACKNOWLEDGMENTS

This research was funded by the Agencia Nacional de Investigación y Desarrollo (ANID), Beca Chile/2019-72200251 and the Nederlandse Organisatie voor Wetenschappelijk Onderzoek (NWO), project number OCENW.M.22.375 (Where and when is water moving in soil? Incorporating spatiotemporal variability of subsurface flows to improve hydrological modelling). The field experiment was funded by ANID, FONDECYT project number 1191057. We thank professor Dr. José Dörner, director of the FONDECYT project 1191057, for kindly providing this data set.

CONFLICT OF INTEREST STATEMENT

The authors declare no conflicts of interest.

DATA AVAILABILITY STATEMENT

Data will be available upon request

ORCID

Sebastián Bravo Peña https://orcid.org/0009-0005-3970-6187
Loes van Schaik https://orcid.org/0000-0002-5742-2859
José Dörner https://orcid.org/0000-0003-4016-2875
Jos van Dam https://orcid.org/0000-0002-3369-0875

REFERENCES

Basile, A., Ciollaro, G., & Coppola, A. (2003). Hysteresis in soil water characteristics as a key to interpreting comparisons of laboratory and field measured hydraulic properties. *Water Resources Research*, *39*(12), 1355. https://doi.org/0.1029/2003WR002432

Basset, C., Abou Najm, M., Ghezzehei, T., Hao, X., & Daccache, A. (2023). How does soil structure affect water infiltration? A meta-data systematic review. *Soil and Tillage Research*, *226*, 105577. https://doi.org/10.1016/j.still.2022.105577

Beck-Broichsitter, S., Gerke, H. H., Leue, M., von Jeetze, P. J., & Horn, R. (2020). Anisotropy of unsaturated soil hydraulic properties of eroded Luvisol after conversion to hayfield comparing alfalfa and grass plots. *Soil and Tillage Research*, *198*, 104553. https://doi.org/10.1016/j.still.2019.104553

Beck-Broichsitter, S., Schroeder, R., Mordhorst, A., Fleige, H., & Horn, R. (2023). Soil water diffusivity as function of the pore size distribution and precompression stress. *Soil and Tillage Research*, *229*, 105675. https://doi.org/10.1016/j.still.2023.105675

Beven, K., & Germann, P. (2013). Macropores and water flow in soils revisited. *Water Resources Research*, *49*(6), 3071–3092. https://doi.org/10.1002/wrcr.20156

Blöschl, G., & Sivapalan, M. (1995). Scale issues in hydrological modelling: A review. *Hydrological Processes*, *9*(3–4), 251–290. https://doi.org/10.1002/hyp.3360090305

Blume, T., Zehe, E., & Bronstert, A. (2008). Investigation of runoff generation in a pristine, poorly gauged catchment in the Chilean Andes II: Qualitative and quantitative use of tracers at three spatial scales. *Hydrological Processes*, *22*(18), 3676–3688. https://doi.org/10.1002/hyp.6970

Blume, T., Zehe, E., & Bronstert, A. (2009). Use of soil moisture dynamics and patterns at different spatio-temporal scales for the investigation of subsurface flow processes. *Hydrology and Earth System Sciences*, *13*(7), 1215–1233. https://doi.org/10.5194/hess-13-1215-2009

Bodner, G., Scholl, P., & Kaul, H. P. (2013). Field quantification of wetting–drying cycles to predict temporal changes of soil pore size distribution. *Soil and Tillage Research*, *133*, 1–9. https://doi.org/10.1016/j.still.2013.05.006

Bonetti, S., Wei, Z., & Or, D. (2021). A framework for quantifying hydrologic effects of soil structure across scales. *Communications Earth & Environment*, *2*(1), 107. https://doi.org/10.1038/s43247-021-00180-0

Bravo, S., Gonzalez-Chang, M., Dec, D., Valle, S., Wendroth, O., Zuniga, F., & Dorner, J. (2020). Using wavelet analyses to identify temporal coherence in soil physical properties in a volcanic ash-derived soil. *Agricultural and Forest Meteorology*, *285*, 107909. https://doi.org/10.1016/j.agrformet.2020.107909

Brooks, R. H., & Corey, A. T. (1966). Properties of porous media affecting fluid flow. *Journal of the Irrigation and Drainage Division*, *92*(2), 61–88. https://doi.org/10.1061/JRCEA4.0000425

Burdine, N. (1953). Relative permeability calculations from pore size distribution data. *Journal of Petroleum Technology*, *5*(03), 71–78.

Dec, D., Bravo, S., Clunes, J., Granda, S., López, I. F., Ordóñez, I., Zúñiga, F., & Dörner, J. (2022). The role of the specific properties of an Andosol as a water reservoir to improve pasture growth and prevent soil physical degradation in irrigated grazing systems. *Journal of Soil Science and Plant Nutrition*, *22*(3), 3756–3773. https://doi.org/10.1007/s42729-022-00925-6

Dec, D., Zúñiga, F., Thiers, O., Paulino, L., Valle, S., Villagra, V., Tadich, I., Horn, R., & Dörner, J. (2017). Water and temperature dynamics of Aquands under different uses in southern Chile. *Journal of Soil Science and Plant Nutrition*, *17*(1), 141–154. https://doi.org/10.4067/S0718-95162017005000011

Diamantopoulos, E., Iden, S. C., & Durner, W. (2012). Inverse modeling of dynamic nonequilibrium in water flow with an effective approach. *Water Resources Research*, *48*(3), W03503. https://doi.org/10.1029/2011WR010717

Dörner, J., Bravo, S., Clunes, J., Horn, R., Dec, D., Valle, S., Zuñiga, F., Wendroth, O., & Werth, J. (2023). Assessing temporal changes of the soil mechanical strength of a volcanic ash soil at different bulk densities under pasture. *Journal of Soil Science and Plant Nutrition*, *23*(2), 2007–2017. https://doi.org/10.1007/s42729-023-01155-0

Dörner, J., Dec, D., Peng, X., & Horn, R. (2009). Change of shrinkage behavior of an Andisol in southern Chile: Effects of land use and wetting/drying cycles. *Soil & Tillage Research*, *106*, 45–53. https://doi.org/10.1016/j.still.2009.09.013

Dörner, J., Dec, D., Peng, X., & Horn, R. (2010). Effect of land use change on the dynamic behaviour of structural properties of an Andisol in southern Chile under saturated and unsaturated hydraulic conditions. *Geoderma*, *159*(1–2), 189–197. https://doi.org/10.1016/j.geoderma.2010.07.011

Dörner, J., Huertas, J., Cuevas, J. G., Leiva, C., Paulino, L., & Arumí, J. L. (2015). Water content dynamics in a volcanic ash soil slope in southern Chile. *Journal of Soil Science and Plant Nutrition*, *178*(4), 693–702. https://doi.org/10.1002/jpln.201500112

Dörner, J., Bravo, S., Stoorvogel, M., Dec, D., Valle, S., Clunes, J., Horn, R., Uteau, D., Wendroth, O., Lagos, L., & Zúñiga, L. (2022). Short-term effects of compaction on soil mechanical properties and pore functions of an Andisol. *Soil & Tillage Research*, *221*, 105396. https://doi.org/10.1016/j.still.2022.105396

Durner, W. (1994). Hydraulic conductivity estimation for soils with heterogeneous pore structure. *Water Resources Research*, *30*(2), 211–223. https://doi.org/10.1029/93WR02676

Eagleson, P. S. (1994). The evolution of modern hydrology (from watershed to continent in 30 years). *Advances in Water Resources*, *17*(1), 3–18. https://doi.org/10.1016/0309-1708(94)90019-1

Ellies, A., Ramírez, C., & Mac Donald, R. (2005). Organic matter and wetting capacity distribution in aggregates of Chilean soils. *Catena*, *59*(1), 69–78. https://doi.org/10.1016/j.catena.2004.05.005

Fatichi, S., Or, D., Walko, R., Vereecken, H., Young, M. H., Ghezzehei, T. A., Hengl, T., Kollet, S., Agam, N., & Avissar, R. (2020). Soil structure is an important omission in Earth System Models. *Nature Communications*, *11*(1), 522. https://doi.org/10.1038/s41467-020-14411-z

González-Reyes, A., & Muñoz, A. (2013). Cambios en la precipitación de la ciudad de Valdivia (Chile) durante los últimos 150 años. *Bosque*, *34*(2), 191–200. https://doi.org/10.4067/S0717-92002013000200008

Haines, W. B. (1930). Studies in the physical properties of soil. V. The hysteresis effect in capillary properties, and the modes of moisture distribution associated therewith. *The Journal of Agricultural Science*, *20*(1), 97–116. https://doi.org/10.1017/S002185960008864X

Hannes, M., Wollschläger, U., Schrader, F., Durner, W., Gebler, S., Pütz, T., Fank, J., von Unold, G., & Vogel, H. J. (2015). A comprehensive filtering scheme for high-resolution estimation of the water balance components from high-precision lysimeters. *Hydrology and Earth System Sciences*, *19*(8), 3405–3418. https://doi.org/10.5194/hess-19-3405-2015

Hannes, M., Wollschläger, U., Wöhling, T., & Vogel, H.-J. (2016). Revisiting hydraulic hysteresis based on long-term monitoring of hydraulic states in lysimeters. *Water Resources Research*, *52*(5), 3847–3865. https://doi.org/10.1002/2015WR018319

Hartge, K. H., Horn, R., Horton, R., Bachmann, J., & Peth, S. (2016). *Essential soil physics. An introduction to soil processes, structure, and mechanics*. Schweizerbart Science Publishers.

Hendrickx, M. G. A., Diels, J., Janssens, P., Schlüter, S., & Vanderborght, J. (2023). Temporal covariance of spatial soil moisture variations: A mechanistic error modeling approach. *Vadose Zone Journal*, *23*(3), e20295. https://doi.org/10.1002/vzj2.20295

Herbrich, M., & Gerke, H. H. (2017). Scales of water retention dynamics observed in eroded Luvisols from an arable postglacial soil landscape. *Vadose Zone Journal*, *16*(10), 1–17. https://doi.org/10.2136/vzj2017.01.0003

Hohenbrink, T. L., Jackisch, C., Durner, W., Germer, K., Iden, S. C., Kreiselmeier, J., Leuther, F., Metzger, J. C., Naseri, M., & Peters, A. (2023). Soil water retention and hydraulic conductivity measured in a wide saturation range. *Earth System Science Data*, *15*(10), 4417–4432. https://doi.org/10.5194/essd-15-4417-2023

Horn, R., Peng, X., Fleige, H., & Dörner, J. (2014). Pore rigidity in structured soils—Only a theoretical boundary condition for hydraulic properties? *Soil Science and Plant Nutrition*, *60*(1), 3–14. https://doi.org/10.1080/00380768.2014.886159

Huang, X., Wang, H., Zhang, M., Horn, R., & Ren, T. (2021). Soil water retention dynamics in a Mollisol during a maize growing season under contrasting tillage systems. *Soil and Tillage Research*, *209*, 104953. https://doi.org/10.1016/j.still.2021.104953

Jarvis, N., Coucheney, E., Lewan, E., Klöffel, T., Meurer, K. H. E., Keller, T., & Larsbo, M. (2024). Interactions between soil structure dynamics, hydrological processes, and organic matter cycling: A new soil-crop model. *European Journal of Soil Science*, *75*(2), e13455. https://doi.org/10.1111/ejss.13455

Jarvis, N., Koestel, J., & Larsbo, M. (2016). Understanding preferential flow in the vadose zone: Recent advances and future prospects. *Vadose Zone Journal*, *15*(12), 1–11. https://doi.org/10.2136/vzj2016.09.0075

Kosugi, K. (1996). Lognormal distribution model for unsaturated soil hydraulic properties. *Water Resources Research*, *32*(9), 2697–2703. https://doi.org/10.1029/96WR01776

Kulli, B., Gysi, M., & Flühler, H. (2003). Visualizing soil compaction based on flow pattern analysis. *Soil and Tillage Research*, *70*(1), 29–40. https://doi.org/10.1016/S0167-1987(02)00121-6

Marquardt, D. W. (1963). An algorithm for least-squares estimation of nonlinear parameters. *Journal of the Society for Industrial and Applied Mathematics*, *11*(2), 431–441.

Mosquera, G. M., Franklin, M., Jan, F., Rolando, C., Lutz, B., David, W., & Patricio, C. (2021). A field, laboratory, and literature review evaluation of the water retention curve of volcanic ash soils: How well do standard laboratory methods reflect field conditions? *Hydrological Processes*, *35*(1), e14011. https://doi.org/10.1002/hyp.14011

Mualem, Y. (1976). A new model for predicting the hydraulic conductivity of unsaturated porous media. *Water Resources Research*, *12*(3), 513–522. https://doi.org/10.1029/WR012i003p00513

Nimmo, J. R. (2021). The processes of preferential flow in the unsaturated zone. *Soil Science Society of America Journal*, *85*(1), 1–27. https://doi.org/10.1002/saj2.20143

Pečan, U., Pintar, M., Mihelič, R., & Kastelec, D. (2023). Variability of in situ soil water retention curves under different tillage systems and growing seasons. *Soil and Tillage Research*, *233*, 105779. https://doi.org/10.1016/j.still.2023.105779

Peng, X., & Horn, R. (2005). Modeling soil shrinkage curve across a wide range of soil types. *Soil Science Society of America Journal*, *69*(3), 584–592. https://doi.org/10.2136/sssaj2004.0146

Peters, A., Nehls, T., Schonsky, H., & Wessolek, G. (2014). Separating precipitation and evapotranspiration from noise—a new filter routine for high-resolution lysimeter data. *Hydrology and Earth System Sciences*, *18*(3), 1189–1198. https://doi.org/10.5194/hess-18-1189-2014

Posit team. (2023). *RStudio: Integrated development environment for R. Posit software, PBC*. http://www.posit.co/

Poulovassilis, A. (1962). Hysteresis of pore water, an application of the concept of independent domains. *Soil Science*, *93*(6), 405–412. https://journals.lww.com/soilsci/fulltext/1962/06000/hysteresis_of_pore_water,_an_application_of_the.7.aspx

Ritsema, C. J., van Dam, J. C., Dekker, L. W., & Oostindie, K. (2005). A new modelling approach to simulate preferential flow and transport in water repellent porous media: Model structure and validation. *Soil Research*, *43*(3), 361–369. https://doi.org/10.1071/SR05054

Rosenbaum, U., Bogena, H. R., Herbst, M., Huisman, J. A., Peterson, T. J., Weuthen, A., Western, A. W., & Vereecken, H. (2012). Seasonal and event dynamics of spatial soil moisture patterns at the small catchment scale. *Water Resources Research*, *48*, W10544. https://doi.org/10.1029/2011WR011518

Seguel, O., & Horn, R. (2006). Structure properties and pore dynamics in aggregate beds due to wetting–drying cycles. *Journal of Plant Nutrition and Soil Science*, *169*(2), 221–232. https://doi.org/10.1002/jpln.200521854

Seki, K., Toride, N., & th. van Genuchten, M. (2022). Closed-form hydraulic conductivity equations for multimodal unsaturated soil hydraulic properties. *Vadose Zone Journal*, *21*(1), e20168. https://doi.org/10.1002/vzj2.20168

Seki, K., Toride, N., & van Genuchten, M. T. (2023). Evaluation of a general model for multimodal unsaturated soil hydraulic properties. *Journal of Hydrology and Hydromechanics*, *71*(1), 22–34. https://doi.org/10.2478/johh-2022-0039

Šimůnek, J., Jarvis, N. J., van Genuchten, M. T., & Gärdenäs, A. (2003). Review and comparison of models for describing non-equilibrium and preferential flow and transport in the vadose zone. *Journal of Hydrology*, *272*(1), 14–35. https://doi.org/10.1016/S0022-1694(02)00252-4

van Genuchten, M. T. (1980). A closed-form equation for predicting the hydraulic conductivity of unsaturated soils. *Soil Science Society of America Journal*, *44*(5), 892–898. https://doi.org/10.2136/sssaj1980.03615995004400050002x

van Schaik, N. L. M., Hendriks, R., & Van Dam, J. (2010). Parameterization of macropore flow using dye-tracer infiltration patterns in the SWAP model. *Vadose Zone Journal*, *9*(1), 95–106. https://doi.org/10.2136/vzj2009.0031

van Schaik, N. L. M. B., Schnabel, S., & Jetten, V. G. (2008). The influence of preferential flow on hillslope hydrology in a semi-arid watershed (in the Spanish Dehesas). *Hydrological Processes*, *22*(18), 3844–3855. https://doi.org/10.1002/hyp.6998

Vereecken, H., Amelung, W., Bauke, S. L., Bogena, H., Brüggemann, N., Montzka, C., Vanderborght, J., Bechtold, M., Blöschl, G., Carminati, A., Javaux, M., Konings, A. G., Kusche, J., Neuweiler, I., Or, D., Steele-Dunne, S., Verhoef, A., Young, M., & Zhang, Y. (2022). Soil hydrology in the Earth system. *Nature Reviews Earth & Environment*, *3*(9), 573–587. https://doi.org/10.1038/s43017-022-00324-6

Vogel, H.-J., Gerke, H. H., Mietrach, R., Zahl, R., & Wöhling, T. (2023). Soil hydraulic conductivity in the state of nonequilibrium. *Vadose Zone Journal*, *22*(2), e20238. https://doi.org/10.1002/vzj2.20238

Vogel, T., van Genuchten, M. T., & Cislerova, M. (2000). Effect of the shape of the soil hydraulic functions near saturation on variably-saturated flow predictions. *Advances in Water Resources*, *24*(2), 133–144. https://doi.org/10.1016/S0309-1708(00)00037-3

Wang, F., Wang, G., Cui, J., Guo, L., Tang, X., Yang, R., & Huang, K. (2023). Hillslope-scale variability of soil water potential over humid alpine forests: Unexpected high contribution of time-invariant component. *Journal of Hydrology*, *617*, 129036. https://doi.org/10.1016/j.jhydrol.2022.129036

Weber, T. K. D., Weihermüller, L., Nemes, A., Bechtold, M., Degré, A., Diamantopoulos, E., Fatichi, S., Filipović, V., Gupta, S., Hohenbrink, T. L., Hirmas, D. R., Jackisch, C., De Jong Van Lier, Q., Koestel, J., Lehmann, P., Marthews, T. R., Minasny, B., Pagel, H., Van Der Ploeg, M., … Bonetti, S. (2024). Hydro-pedotransfer functions: A roadmap for future development. *Hydrology and Earth System Sciences*, *28*(14), 3391–3433. https://doi.org/10.5194/hess-28-3391-2024

WRB, I. W. G. (2014). *World Reference Base for soil resources 2014: International soil classification system for naming soils and creating legends for soil maps*. World Soil Resources Report No. 106. FAO, Rome. https://publications.jrc.ec.europa.eu/repository/handle/JRC91947

Zhang, M., Lu, Y., Heitman, J., Horton, R., & Ren, T. (2017). Temporal changes of soil water retention behavior as affected by wetting and drying following tillage. *Soil Science Society of America Journal*, *81*(6), 1288–1295. https://doi.org/10.2136/sssaj2017.01.0038

SUPPORTING INFORMATION

Additional supporting information can be found online in the Supporting Information section at the end of this article.

How to cite this article: Bravo Peña, S., van Schaik, L., Dörner, J., & van Dam, J. (2025). Dynamic soil water retention properties: Exploring the interplay of moisture states and soil structure dynamics in a compacted Andosol. *Vadose Zone Journal*, *24*, e70021. https://doi.org/10.1002/vzj2.70021